



# **Tectono-metamorphic history of the eastern Taureau shear zone, Mauricie area, Québec: Implications for the exhumation of the mid-crust in the Grenville Province**

Renaud Soucy La Roche, Félix Gervais, Alain Tremblay, James L. Crowley,  
Gilles Ruffet

## **► To cite this version:**

Renaud Soucy La Roche, Félix Gervais, Alain Tremblay, James L. Crowley, Gilles Ruffet. Tectono-metamorphic history of the eastern Taureau shear zone, Mauricie area, Québec: Implications for the exhumation of the mid-crust in the Grenville Province. *Precambrian Research*, 2015, 257, pp.22-46. 10.1016/j.precamres.2014.11.012 . insu-01096499

**HAL Id: insu-01096499**

**<https://insu.hal.science/insu-01096499>**

Submitted on 7 Jan 2015

**HAL** is a multi-disciplinary open access archive for the deposit and dissemination of scientific research documents, whether they are published or not. The documents may come from teaching and research institutions in France or abroad, or from public or private research centers.

L'archive ouverte pluridisciplinaire **HAL**, est destinée au dépôt et à la diffusion de documents scientifiques de niveau recherche, publiés ou non, émanant des établissements d'enseignement et de recherche français ou étrangers, des laboratoires publics ou privés.

TECTONO-METAMORPHIC HISTORY OF THE EASTERN TAUREAU SHEAR ZONE, MAURICIE AREA, QUÉBEC:  
IMPLICATIONS FOR THE EXHUMATION OF THE MID-CRUST IN THE GRENVILLE PROVINCE

SOUCY LA ROCHE, Renaud<sup>a1</sup>, GERVAIS, Félix<sup>b</sup>, TREMBLAY, Alain<sup>c</sup>, CROWLEY, James L.<sup>d</sup>, RUFFET, Gilles<sup>e</sup>

Corresponding author:

<sup>a</sup> Département des Sciences de la Terre et de l'Atmosphère and GEOTOP, Université du Québec à Montréal, C.P. 8888, succursale Centre-Ville, Montréal, Québec, Canada, H3C 3P8. soucy\_la\_roche.renaud@courrier.uqam.ca, +1 438-391-2923.

<sup>b</sup> Département des Génies Civil, Géologique et des Mines, École Polytechnique de Montréal, C.P. 6079, succursale Centre-Ville, Montréal, Québec, Canada, H3C 3A7. felix.gervais@polymtl.ca

<sup>c</sup> Département des Sciences de la Terre et de l'Atmosphère and GEOTOP, Université du Québec à Montréal, C.P. 8888, succursale Centre-Ville, Montréal, Québec, Canada, H3C 3P8. tremblay.a@uqam.ca

<sup>d</sup> Department of Geosciences, Boise State University, 1910 University Drive, Boise, Idaho, USA, 83725-1535. jimcrowley@boisestate.edu

<sup>e</sup> Géosciences Rennes, UMR CNRS 6118, Université de Rennes 1, Campus de Beaulieu, 35042 Rennes Cedex, France. gilles.ruffet@univ-rennes1.fr

Present address:

<sup>1</sup> Department of Geological Sciences & Geological Engineering, 36 Union Street, Queen's University, Kingston, Ontario, Canada, K7L 3N6. 13rslr@queensu.ca. +1 438-391-2923.

## Abstract

This study investigates the tectono-metamorphic history and exhumation mechanisms of the mid-crustal Mékinac-Taureau domain of the Mauricie area, central Grenville Province. Macro- and micro-structural analyses reveal the top-down-to-the-ESE sense of shear on the eastern Taureau shear zone, a major extensional structure that exhumed the mid-crustal Mékinac-Taureau domain and juxtaposed it against the lower grade rocks of the Shawinigan domain. Peak metamorphism in the Mékinac-Taureau domain, inferred to be the result of northwestward thrusting and regional crustal thickening, took place under P-T conditions of 1000-1100 MPa and 820-880 °C prior to  $1082 \pm 20$  Ma. Retrograde conditions varying from 775 to 675 °C and from 800 to 650 MPa were registered in its upper structural levels prior to and/or during shearing along the eastern Taureau shear zone that was active at  $1064 \pm 15$  Ma. The Shawinigan domain records P-T conditions ranging from 850 to 625 MPa and from 775 to 700 °C, P-T values that are similar to or slightly lower than those for retrogressed samples from the upper structural levels of the Mékinac-Taureau domain, but clearly lower than the peak metamorphism values of the latter domain. Finally, the area cooled below 550-600 °C at  $\sim 1000$ -1030 Ma and below 450 °C at  $\sim 900$ -970 Ma on the basis of  $^{40}\text{Ar}/^{39}\text{Ar}$  geochronology on amphibole and biotite. Structural and metamorphic characteristics of the Mauricie area are similar to those expected from a metamorphic core complex formed during post-convergence orogenic collapse in a gravity-driven fixed-boundary mode. The Mékinac-Taureau and Shawinigan domains were thus probably exhumed by a similar process, which supports the orogenic collapse model recently proposed to explain the exhumation of mid-crustal metamorphic core complexes in the Grenville Province.

Keywords: Grenville Province; Eastern Taureau shear zone; Middle crust exhumation; Geochronology; Thermobarometry

44

45 **1. Introduction**

46 In collisional orogens, the mechanisms by which high-grade metamorphic rocks are exhumed (i.e.  
47 displaced towards Earth's surface; England and Molnar, 1990) by mechanisms are central to many  
48 debates (e.g. Gapais et al., 2009; Gervais and Brown, 2011; Ring et al., 1999). For instance, mid-crustal  
49 units can be exhumed by syn-convergent channel flow coupled to focused erosion (e.g. Beaumont et al.,  
50 2001, 2006), by post-convergent orogenic collapse (e.g. Dewey, 1988; Rey et al., 2001) and associated  
51 metamorphic core complexes (MCC) development (e.g. Brun et al., 1994; Rey et al., 2009; Tirel, 2004;  
52 Tirel et al., 2004, 2006, 2008), by diapirism (e.g. Calvert et al., 1999; Teyssier and Whitney, 2002), and in  
53 orogenic wedges whose shape is described by the critical taper theory (e.g. Dahlen, 1990; Platt, 1986).

54 These mechanisms have all been proposed to explain the exhumation of mid-crustal units during  
55 the late Mesoproterozoic to early Neoproterozoic Grenvillian orogeny. The Grenville Province  
56 represents the southeastern boundary of Proterozoic Laurentia and the Grenvillian orogeny is  
57 characterized by a >100 m.y. period of heating and crustal thickening that affected a wide area of  
58 reworked Laurentian orogenic crust (>600 km; Hynes and Rivers, 2010; Rivers, 2008, 2009, 2012; Rivers  
59 et al. 2012). Recent work demonstrated that the orogenic crust can be subdivided into lower, mid and  
60 upper crustal segments (Rivers, 2008, 2012 and references therein), contrasting with the long-lasting  
61 interpretation of this province as a homogeneous slice through the mid-crust, and thus promoting  
62 research on orogenic collapse mechanisms. Following the idea of Dewey (1988), Rivers (2008) suggested  
63 the presence of a Tibetan-type orogenic plateau in the hinterland of the orogeny that resulted from  
64 thickening of the continental crust. In such a setting, the mid-crust is typically weakened by partial  
65 melting at depth (Rosenberg and Handy, 2005) and may flow laterally (Rey et al., 2001; Royden, 1996;  
66 Vanderhaeghe et al., 2003). The importance of ductile flow in the mid-crust of the Grenville orogen was  
67 assessed recently (Jamieson et al., 2007, 2010; Rivers, 2008, 2009), and a heterogeneous channel flow  
68 model, in which the weak ductile layer is thrust above a strong indentor, was proposed (Jamieson et al.,  
69 2007, 2010). A complementary model of exhumation (Rivers, 2008, 2012) presents the Grenville  
70 Province as a series of high-grade mid-crustal core complexes overlaid by fragments of the upper crust  
71 resulting from the collapse of the orogenic plateau, following crustal thickening and mid-crustal flow.  
72 Multiple regions of the Grenville Province that exhibit normal-sense faults and shear zones juxtaposing

the potential mid-crustal core complexes with upper crustal segments were recognized by Rivers (2008, 2009, 2012). These regions include large parts of the northeastern Grenville Province, the southeastern Composite Arc Belt, the northwestern Frontenac-Adirondack Belt and smaller areas such as the Natashquan domain and the Mauricie area (Fig. 1). Finally, in a few specific localities in the eastern Grenville Province, diapirism has been proposed to explain the exhumation of high grade gneiss domes (e.g. Gervais et al., 2004), and the orogenic wedge model has been invoked to explain the formation and exhumation of a mid-crustal foreland fold-thrust belt (van Gool et al., 2008).

This contribution presents new data from the Mauricie area to further investigate the exhumation of a mid-crustal high-grade gneiss dome known as the Mékinac-Taureau domain (Nadeau and Brouillette, 1994, 1995). Detailed macro- and micro-structural analyses reveal the kinematic history of the eastern Taureau shear zone (TSZ), a major regional structure responsible for the exhumation of the Mékinac-Taureau domain. Thermobarometry was applied to six selected samples in order to evaluate the peak pressure and temperature (P-T) conditions and the retrograde path of the Mékinac-Taureau and overlying Shawinigan domains. Both the timing of peak metamorphism and exhumation were constrained by U-Pb geochronology on zircon from two pegmatite dykes.  $^{40}\text{Ar}/^{39}\text{Ar}$  thermochronology on amphibole and biotite separates from six samples was undertaken to provide precise timing constraints for the cooling of this area through the closure temperatures of these minerals. These structural, thermobarometric and geochronologic constraints were then compared with equivalent data determined from type localities in well-known orogenic belts or predicted by analog/numerical modeling of different exhumation processes to constrain the most likely process for the Mauricie area.

## 2. Geological setting

The Grenville Province comprises rocks of southeastern Laurentia that were affected by multiple orogenic events from late Paleoproterozoic until early Neoproterozoic (Hynes and Rivers, 2010; Rivers, 1997; Rivers et al. 2012). The Grenvillian orogeny is the youngest of these and can be separated into two main phases according to their age and spatial extent (Rivers, 1997, 2008; Rivers et al. 2012). The Ottawa phase affected the hinterland of the Grenville Province during a first pulse of compression from 1090 to 1020 Ma. The rocks affected by this orogenic phase are far-travelled with respect to the Laurentian margin and are referred to as allochthonous belts. This contrasts with the structurally underlying parautochthonous belt, located to the northwest, which comprises rocks of the Laurentian

margin that can be correlated with the Grenvillian foreland in the adjacent Archean and Proterozoic Superior provinces. The latter belt was deformed and metamorphosed during a second phase of compression, known as the Rigolet, between 1000 and 980 Ma. Rivers (2008, 2012) subdivided the allochthonous hinterland affected by the Ottawa orogeny into four belts according to their relative positions in the crust (Fig. 1). From base to top, (1) the allochthonous high-pressure belt (aHP Belt) comprises nappes of relict eclogitic material overprinted by granulite-facies metamorphism. The aHP belt is directly underlain by the Allochthon Boundary Thrust in two areas of the western and central Grenville Province. The aHP belt represents remnants of the base of the doubly-thickened orogenic crust that have been incorporated into the mid crust during their exhumation. (2) The allochthonous medium-pressure belt (aMP Belt) is the most extensive belt, extending along the whole length of the Grenville Province. It is composed of upper amphibolite- to granulite-facies mid-crustal units of various compositions that are commonly migmatitic. The upper crust is preserved as two distinct levels, (3) the allochthonous low-pressure belt (aLP Belt) and (4) the Ottawa Orogenic Lid (OOL). The aLP Belt is exposed only in small areas of the southeastern, central and western Grenville Province. It consists of greenschist to amphibolite-facies rocks that were juxtaposed to the aMP Belt via extensional shear zones. Finally, the structurally overlying OOL occupies large zones of the northeast and southwest Grenville Province. It comprises units that escaped penetrative Ottawa metamorphism and deformation, although they may have been subjected to older tectono-metamorphic episodes.

### 3. Regional geology

The present study is located in the Mauricie area, central Grenville Province, comprising rocks of the aMP and aLP belts that have been subdivided into three main lithotectonic domains (Figs. 1 and 2; Nadeau and Brouillette, 1994, 1995; Nadeau and Corrigan, 1991). (1) The domal-shaped Mékinac-Taureau domain is the structurally lowest domain that extends for more than 80 km from the St. Maurice River to the Taureau Reservoir. Its northern boundary is not yet recognized, but it is in tectonic contact to the west, south and south-east with the overlying Morin Terrane along the TSZ. (2) The Morin Terrane is principally exposed on the western side of the Mékinac-Taureau domain, but a thin slice of this terrane extends towards the east where it is referred to as the Shawinigan domain (e.g. Corrigan, 1995; Corrigan and van Breemen, 1997; Rivers, 2008). (3) To the east, the elongate, north-south striking Portneuf-Mauricie domain structurally overlies the two other lithotectonic domains along the

Tawachiche shear zone. These three lithotectonic domains can be distinguished according to their lithology, age, structural style and magnetic signature (Corrigan, 1995; Nadeau and Brouillette, 1994, 1995; Nadeau and Corrigan, 1991).

### 3.1. Lithotectonic domains

#### 3.1.1 Mékinac-Taureau domain

The Mékinac-Taureau domain is mostly composed of ~1370 Ma granodioritic orthogneiss (age from Nadeau and van Breemen, unpublished data, reported in Corrigan and van Breemen, 1997) that forms part of the aMP Belt of Rivers (2008). It is mostly at granulite facies, but upper amphibolite-facies gneiss occurs in the Reservoir Taureau area of the Mékinac-Taureau domain (Nadeau and Brouillette, 1995). According to Corrigan and van Breemen (1997), the metamorphism occurred from 1120 to 1090 Ma and was due to crustal thickening during northwestward thrusting structurally above the present exposure of units.

The Mékinac-Taureau domain orthogneiss is generally homogeneous on the map scale, but varies between granodioritic, granitic, dioritic and gabbroic compositions in any one outcrop (Nadeau and Brouillette, 1995). Felsic and intermediate gneiss is pervasively migmatitic, whereas migmatitic mafic gneiss is only locally present. Rare, discontinuous layers of quartzite, calc-silicate gneiss, marble and Sil-Kfs-Grt-bearing, migmatitic metapelite, commonly concordant to the regional foliation, are found close to the eastern margin of the Mékinac-Taureau domain (mineral abbreviations after Kretz, 1983).

Field observations in this study confirmed the general structural pattern outlined on Nadeau and Brouillette's (1994, 1995) compilation maps. A regional foliation ( $S_n$ ), defined by preferred orientation of minerals, ribbon quartz, gneissic compositional banding and stromatic layers of leucosome, gently dips towards the margins of the domain, although local variations occur (Fig. 2). In the interior of the domain, marble layers record high qualitative strain, as evidenced by numerous sheath folds and contorted to rounded fragments of country rocks. They were interpreted as tectonic breccias by Nadeau and Brouillette (1995). Hanmer (1988) attributed similar structures to the relatively low viscosity of marble at high temperature and pressure as compared to the surrounding gneiss. The stretching and mineral lineations ( $L_n$ ) are generally poorly developed in the interior of the domain (Fig. 2). On the southern and southeastern boundaries, a well-developed stretching lineation plunges gently to moderately (10-35°) to the ESE ( $L_{n+1}$ ) (Fig. 2). A third population of lineation ( $L_{n+2}$ ) plunging gently (0-20°) to the NE is recognized

on the eastern side along the Tawachiche shear zone (Fig. 2). Geochronological constraints suggest that  $L_{n+1}$  is younger than  $L_n$  (see section 6), whereas cross-cutting relationships imply that  $L_{n+2}$  is younger than  $L_n$  (Nadeau and Brouillette, 1994). However, there is no clear cross-cutting relationship between  $L_{n+1}$  and  $L_{n+2}$ , thus this notation does not imply an age sequence.

### 3.1.2. Morin Terrane (including the Shawinigan domain)

The Morin Terrane comprises granulite-facies gneiss and plutonic complexes belonging to the aMP Belt (Rivers, 2008). The western side of the Morin Terrane comprises ~1330 Ma orthogneiss (Peck, 2012), amphibolite, quartzofeldspathic gneiss, paragneiss, quartzite and marble (Martignole, 1975) metamorphosed at granulite-facies prior to the intrusion of the Morin and Lac Croche plutonic complexes (1165-1135 Ma; Barton and Doig, 1972; Doig, 1991; Friedman and Martignole, 1995). A second granulite-facies metamorphic event followed the intrusions, but is otherwise temporally unconstrained (Peck et al., 2005). In contrast to the granulite-facies west-side, the eastern side of the Morin Terrane, referred to as the Shawinigan domain, is characterized by the presence of upper amphibolite-facies rocks (Corrigan, 1995; Lévesque, 1995). The metamorphism is coeval with the 1120-1090 Ma metamorphism in the Mékinac-Taureau domain (Corrigan and van Breemen, 1997).

The Shawinigan domain is composed of two major rock units in tectonic contact: felsic to intermediate orthogneiss of the Jésuite complex and the overlying St. Boniface paragneiss. Orthogneiss of the Jésuite complex is mainly tonalitic in composition, with a crystallization age of ~1370 Ma (Corrigan and van Breemen, 1997), but granitic and rare gabbroic rocks are present locally. Stromatic migmatite is common, although not as pervasive as it is in the upper structural levels of the Mékinac-Taureau domain. The St. Boniface paragneiss comprises mainly Sil-Kfs-Grt-bearing, migmatitic metapelite with minor quartzite and marble that were deposited after 1180 Ma on the basis of limited detrital zircon data (Corrigan and van Breemen, 1997).

Important masses of anorthosite-mangerite-charnockite-granite (AMCG), gabbro, porphyritic granite and monzonite intruded the Morin Terrane during two episodes of magmatism (Corrigan and van Breemen, 1997). The first episode includes the 1165-1135 Ma Morin anorthositic complex (Doig, 1991; Friedman and Martignole, 1995), the ~1140 Ma Lac Croche complex (Barton and Doig, 1972) and the 1153 Ma Lake Paul granite (Corrigan and van Breemen, 1997). The second pulse of magmatism occurred from 1080 to 1056 Ma and includes the Shawinigan norite, the Lejeune complex and the St.



Didace complex (Corrigan and van Breemen, 1997; Nadeau and van Breemen, 2001).

The foliation in the Morin Terrane generally dips away from the contact with the Mékinac-Taureau domain. However, multiple folds described in Nadeau and Brouillette (1995) produce local variations to this trend. The regional structural pattern is also affected by pre-1135 Ma AMGC plutons that are wrapped by the foliation (Martignole, 1975; Nadeau and Brouillette, 1995). In the Shawinigan domain, the foliation ( $S_n$ ) defined by compositional banding dips shallowly to moderately ( $0-45^\circ$ ) to the SE (Fig. 2). The stretching and mineral lineations ( $L_n$ ) plunge sub-horizontally to gently ( $0-15^\circ$ ) to the S and SE (Fig. 2).

### 3.1.3. Portneuf-Mauricie domain

The Portneuf-Mauricie domain comprises the ~1450 Ma Montauban Group supracrustal rocks and the 1400-1370 Ma La Bostonnais calc-alkaline complex plutonic rocks (Corrigan and van Breemen, 1997; Nadeau and Brouillette, 1995; Nadeau and van Breemen, 1994). Rocks of the Portneuf-Mauricie domain are generally at a lower metamorphic grade than the other domains, with middle to upper amphibolite-facies recorded throughout most of the domain, except for the eastern strand where low- to medium-P granulite-facies is observed (Corrigan, 1995; Lévesque, 1995). Metamorphism of the Portneuf-Mauricie domain is associated with the ~1400 Ma pre-Grenvillian accretion of the Montauban Arc and was not overprinted by granulite facies metamorphism during the Grenvillian orogeny, as opposed to the adjacent Mékinac-Taureau and Shawinigan domains (Corrigan, 1995; Corrigan and van Breemen, 1997). Therefore, Rivers (2012) included the Portneuf-Mauricie domain in the aLP Belt.

The structure of the Portneuf-Mauricie domain is characterized by a planar fabric dipping gently to moderately to the SE or E and by two sets of mineral and stretching lineations (Nadeau and Brouillette, 1994, 1995). The first set is pervasive, plunges to the SE and has been attributed to regional NW-directed thrusting (Nadeau and Brouillette, 1995). The second set plunges to the NNE and was developed in discrete shear zones during oblique-sinistral extensional ductile shearing after the peak of metamorphism (Nadeau and Brouillette, 1995).

### 3.2. Lithotectonic boundaries

The contact between the Mékinac-Taureau domain and the Morin Terrane is known as the Taureau shear zone (TSZ; Fig. 1; Martignole and Friedman, 1998). On the western flank of the dome the

shear zone is presumed to be several hundred of meters wide and to gently dip away from the Mékinac-Taureau domain. Martignole and Friedman (1998) proposed oblique thrusting on the TSZ based on local dextral kinematic indicators observed on lineations shallowly plunging to the SE and because of the broad spatial coincidence between the trace of the shear zone and the Opx-in isograd (Schriver, 1973), delimiting granulite-facies rocks of the Morin Terrane from upper amphibolite-facies rocks of the western part of the Mékinac-Taureau domain. They constrained the minimum age of displacement on the TSZ by dating a late-kinematic dyke at  $1074 \pm 4$  Ma. Further east, however, the eastern TSZ does not superpose granulite-facies rocks on top of amphibolite-facies rocks because the Opx-in isograd crosscuts the Mékinac-Taureau domain boundary (Fig 1; Hocq and Dufour, 1999, 2002). In the study area on the eastern flank of the dome, the metamorphic contrast across the TSZ is ambiguous, but previous qualitative observations of metamorphic mineral assemblages and textures, as well as quantitative thermobarometry studies, suggested higher grade in the footwall (Mékinac-Taureau domain) than in the hanging wall (Shawinigan domain) (Corrigan, 1995; Lévesque, 1995; Nadeau and Brouillette, 1995). If the suggested metamorphic contrast is real and if timing of metamorphism is the same for both the Mékinac-Taureau and Shawinigan domains, the two hypotheses are paradoxical: thrusting alone along the eastern TSZ could not explain the present configuration. One objective of the current study is, therefore, to test this hypothesis.

Away from the TSZ, the contact between the Portneuf-Mauricie domain and the Shawinigan domain is marked by an anastomosing array of E-dipping shear zones, collectively known as the Tawachiche shear zone (Fig. 1; Corrigan, 1995; Corrigan and van Breemen 1997; Lemieux, 1992). The total thickness of the area affected by these shear zones may be as wide as 25 km, but most of the shearing occurred directly at the contact between the two domains, along a strand that has an average map width of 1 km (Corrigan, 1995). The Tawachiche shear zone is almost co-planar with the N to NE striking and gently dipping regional foliation of the Portneuf-Mauricie domain. The associated stretching lineation trends to the NNE with a shallow to moderate plunge ( $L_{n+2}$ ). Corrigan (1995) observed a paleopressure offset of 200 to 300 MPa between footwall and hanging wall metamorphic mineral assemblages, with lower pressure in the hanging wall, and therefore suggested that the shear zone accommodated a vertical offset of 7-10 km by top-down-to-the-NNE oblique extensional shearing. Corrigan and van Breemen (1997) constrained the timing of movement along the Tawachiche shear zone between 1065 and 1035 Ma.

#### 4. Structural geology of the eastern TSZ

One of the main objectives of this study was to constrain the kinematic history the TSZ. Field work involved examination of over 200 outcrops from the Mékinac-Taureau domain and the Shawinigan domain, especially in the vicinity of the TSZ. Large (commonly  $>500 \text{ m}^2$ ) and well exposed key outcrops (e.g. Fig. 3A) were studied in detail to document complex structural relationships. Due to poor exposure on the western and south flank of the Mékinac-Taureau domain, the TSZ was only recognized on the eastern flank. Field observations show a general trend from S-tectonites dominant in the interior of the Mékinac-Taureau domain towards S-L and locally L-tectonites developed on its eastern boundary. The opposite variation, that is a transition from S-L-tectonites to S-tectonites, is observed from the boundary structurally up in the Shawinigan domain. As shown on Fig. 2, ESE-trending lineation is abundant and well clustered in the vicinity of the eastern TSZ (domain 3 on Fig. 2) whereas it is only rare and not clustered away from the TSZ. This clearly reveals the presence of the eastern TSZ, which separates the two domains.

The main shear zone is several hundred meters thick and is heterogeneously strained: rock from the TSZ is generally well-foliated and lineated, and locally shows well-developed mylonitic textures that may contain a pre-shearing relict foliation. In the latter case, the relict foliation ( $S_n$ ) is commonly crenulated and folded with axial planes parallel to the new foliation formed in the shear zone ( $S_{n+1}$ , Fig. 3B). The stretching lineation associated with this shear fabric ( $L_{n+1}$ ) plunges gently ( $10\text{-}35^\circ$ ) towards the ESE (Fig. 2). Multiple shear-sense indicators such as  $\sigma$ -porphyroclast,  $\delta$ -porphyroclasts and asymmetric folds (Hanmer and Passchier, 1991) indicate a top-down-to-the-ESE tectonic displacement (Fig. 3C and D). Granitic pegmatites with pre- to syn-kinematic relationships are common in the TSZ. Information about the last increments of strain is provided by the relationship between the pegmatites and crosscutting marble layers of uncertain origin. These layers are of variable thickness (5-200 cm), present a high degree of qualitative strain, contain a foliation and a lineation parallel to those of the host gneiss, and contain clasts of host lithologic units, including pegmatites (Fig. 3A). At their margins, undeformed pegmatites become mylonitic and the entrainment of foliation of the host gneiss indicates a top-down-to-the-ESE sense of shear (Fig. 3E). The marble layers thus accommodated the last strain increments of top-down-to-the-ESE sense of shear along the TSZ (Fig. 3E).

Kinematic indicators attesting to top-down-to-the-ESE sense of shear are also developed locally in

a metapelite layer of the Mékinac-Taureau domain three kilometers structurally below the eastern TSZ. At this locality, quartz ribbons are syn-kinematically recrystallized to form an oblique grain-shape fabric (Passchier and Trouw, 2005; Snoke et al., 1998) (Fig. 4A). This contrasts with the orthogneiss and structurally lower metapelites in which quartz forms fully annealed ribbons.

Finally, in the lower structural levels of the Shawinigan domain, there are multiple ductile-brittle extensional shear zones with a top-down-to-the-SE sense of shear (Fig. 4B). These shear zones probably accommodated only minor displacement because there is no metamorphic or lithological contrasts between the footwall and hanging wall. They may represent structurally higher equivalents of the eastern TSZ that were active during the waning stages of normal shearing.

## 5. Thermobarometry

### 5.1. Qualitative interpretations

Granulite-facies metapelite from both the Mékinac-Taureau and the Shawinigan domains have a similar mineral assemblage composed of Qtz + Kfs + Pl + Grt + Sil + Bt  $\pm$  Rt  $\pm$  Ilm  $\pm$  Zrn  $\pm$  Mnz (Fig. 5A). The presence of Kfs and the absence of Ms, Opx and Ky in the peak assemblage of metapelite constrain the conditions to temperatures higher than the Ms dehydration-melting reaction, below the Opx-in reaction and within the Sil stability field. In felsic to intermediate orthogneiss, the occurrence of migmatitic melt indicates conditions above the wet-solidus of granitic rocks.

There are several differences between the felsic to intermediate orthogneiss units of the Mékinac-Taureau and the Shawinigan domains. Based on our observations in the Mékinac-Taureau domain, the volume of leucosome in rock of felsic and intermediate composition increases structurally upward from only a few percent in the interior of the domain to 20-40% close to upper structural levels. Opx-bearing leucosome occurs in two structural settings. Pre- to syn-deformation leucosome is observed as stromatic layers parallel to the foliation and as pockets of leucosome trapped in boudin necks of more competent mafic layers or in hinges of isoclinal folds, whereas post-deformation leucosome is observed as undeformed, coarse patches that cross-cut the foliation. Because both types of leucosome contain the same mineralogy, and are locally intimately associated (i.e. stromatic leucosome merging into a cross-cutting pocket), our preferred interpretation is that migmatism outlasted the deformation (e.g. Corrigan, 1995). Stromatic leucosome is also observed in the Shawinigan

domain, but to a lesser extent (<20%). The most striking difference is the scarcity of orthopyroxene in Shawinigan domain intermediate orthogneiss (Pl + Qtz + Hbl + Bt  $\pm$  Kfs  $\pm$  Cpx  $\pm$  Opx) and, where present, orthopyroxene in this domain is typically partially retrogressed to hornblende. In the felsic to intermediate orthogneiss (Pl + Qtz + Kfs + Opx + Bt + Hbl) of the Mékinac-Taureau domain, on the other hand, orthopyroxene is abundant and unaltered, especially in the interior of the domain. The wider P-T stability field predicted for orthopyroxene in granodioritic orthogneiss compared to that predicted in metapelite by phase equilibria modeling (Gerya, 2004), most likely explain its presence and absence in the former and latter, respectively. Clinopyroxene is retrogressed to hornblende in intermediate orthogneiss of the Shawinigan domain and only locally in the upper levels of the Mékinac-Taureau domain. This suggests that retrograde metamorphic reactions affected the Shawinigan domain and, to a lesser extent, the Mékinac-Taureau domain. These qualitative observations suggest higher peak metamorphic in the Mékinac-Taureau domain as compared to the Shawinigan domain and/or a more profound retrograde metamorphism in the latter. As a clear metamorphic contrast in peak P-T conditions between the two domains cannot be demonstrated solely on the basis of petrographic observations, quantitative thermobarometry is required.

## 5.2. Analytical methods and strategy

Five metapelite samples and one amphibolite were selected along a transect of approximately ten kilometers of structural thickness to determine the overall metamorphic conditions characterizing the Mékinac-Taureau and Shawinigan domains. Metapelitic samples RS12-021, RS12-015A & RS11-058, as well as RS11-105 & RS12-027B were collected 5.5, 3 & 2.5 km structurally below and 4 & 6 km structurally above the TSZ, respectively. Amphibolite sample RS11-082B was collected within the shear zone (see Fig. 2 for locations). We considered that conventional thermobarometry was the best approach for our samples because: 1) the equilibrium volume chemical compositions to input in phase equilibria modeling would be difficult to estimate because of the heterogeneous texture of the rock; 2) the metapelitic samples do not show textures nor chemical zoning indicative of the retrograde net-transfer reactions that commonly precludes this type of P-T calculations in high-grade metapelite (cf. Spear and Florence, 1992; Spear et al., 1999); 3) amphibolite show textures and chemical zoning susceptible to yield information on the prograde and retrograde path.

Mineral compositions were determined using wavelength-dispersive spectrometry on a JXA JEOL-

8900L microprobe at McGill University. Acceleration voltage was 15 kV, beam current was 20 nA, beam size was 5µm and counting time was 20 seconds. Natural mineral standards were used for calibrations and ZAF correction was used for data reduction. Additional details on standards used and detection limits for the different minerals under above conditions are provided in the supplementary data table 1. Pressure and temperature (P-T) values were calculated with the computer software TWEEQU (Thermobarometry With Estimation of EQUilibrium state) developed by Berman (1991). The TWEEQU version 2.3 (Berman, 2007) was used for calculations on metapelites because it is easier to calculate the classical thermobarometers involving garnet, biotite and plagioclase than with other software such as THERMOCALC, and because it uses a recent thermodynamic database (v2.32, Berman and Aranovich, in prep.) and solution models for garnet (Berman et al., 2007), biotite (Berman et al., 2007) and plagioclase (Fuhrman and Lindsley, 1988). Essene (1989) and Berman (1991) proposed uncertainties of ± 50 °C and ± 100 MPa for P-T calculations using TWEEQU. For the amphibolite, we preferred to use the software THERMOCALC version 3.33 (Holland and Powell, 1998; Powell and Holland, 1988, 1994, 2008) with the thermodynamic dataset ds55 because it uses more recent solution models for amphiboles than TWEEQU (the Dale et al. (2005) model used with AX2 of Holland (2014) vs. the Mäder et al. (1994) model used with TWEEQU v. 1.02). We calculated relative P-T differences and associated uncertainties by calculating the standard deviations of P and T for all permutation of mineral compositions interpreted to have been in equilibrium by using the software TC\_Comp (Dolivo-Dobrovolsky, 2013, <http://www.dimadd.ru/en>), as detailed below.

The following geothermometers and geobarometers were applied:

#### Metapelite



#### Amphibolite



The proper evaluation of P-T conditions in high grade metapelite is a difficult task requiring many precautions (e.g. Spear and Florence, 1992). As several high temperature phenomena may modify the chemical composition of minerals, it is important to evaluate them to make sure that calculated P-T

points are significant. At high temperature (>500-600 °C), the growth zoning pattern of Fe, Mg, Ca and Mn in garnet is modified by intra-crystalline diffusion (e.g. Caddick et al., 2010; Tracy, 1982; Tracy et al., 1976; Yardley, 1977), which depends on the maximum temperature reached, the size of the crystal and the duration of metamorphism. For example, complete homogenization of a garnet with a diameter of 1 mm at temperature reaching 800 °C would require tens of m.y., but the growth zoning pattern would be modified significantly within a few m.y. (Caddick et al., 2010). Inasmuch as the extent of diffusion depends on grain size, P-T calculations on garnet having different diameters should not yield similar values, unless they were completely re-equilibrated. On the other hand, Fe-Mg diffusion in biotite in contact with garnet is effective at >525 °C and at rates much faster than most metamorphic processes (Spear, 1993). Furthermore, Grt-Bt re-equilibration may occur during retrograde metamorphism via exchange reaction (1) and net transfer reaction:



(Kohn and Spear, 2000; Spear, 1993, 2004; Spear and Parrish, 1996; Spear et al., 1999; Tracy, 1982). In addition, the net transfer reaction (7) produces plagioclase and biotite during melt crystallization that may not have compositions reflecting peak P-T conditions. Garnet involved in this reaction generally have embayments and invariably show a spike in Mn at their margins, whereas biotite produced by this reaction have a higher Fe/(Fe + Mg) value than biotite that crystallized at peak conditions. Finally, the rate of Ca diffusion in plagioclase is much slower than the rate of most metamorphic processes; therefore plagioclase composition will only be modified by dissolution and reprecipitation (Grove et al., 1984). Minerals analyzed for peak P-T determination were therefore carefully selected to prevent the inaccuracies introduced by these high temperature phenomena on the calculated P-T points (e.g. Schaub et al., 2002).

Petrographical observations (i.e. lack of muscovite and presence of sillimanite and K-feldspar in metapelite assemblage) suggest high peak temperature (>650 °C). Garnet chemical composition is thus expected to have partially to completely re-equilibrated during peak metamorphism and to possibly have been modified by post-peak metamorphic reactions. Largest available (500 to 4000 µm) garnets were selected because they are likely to preserve a chemical plateau in their cores that would be unaffected by retrograde reactions (Spear et al., 1999; Hauzenberger, 2005). In cases for which garnet did not show a perfectly flat zoning profile in its core, a plateau composition close to the rim was used in

order to avoid the effect of relict growth zoning. Biotite isolated from garnet (e.g. trapped within a non-reacting phase such as quartz or feldspar), with high Ti content (suggestive of higher temperature; Henry et al., 2005), and that was parallel to the foliation (limiting the possibility of analyzing late biotite) was used rather than biotite in contact with garnet to minimize the effect of retrograde re-equilibration. Due to slow Ca diffusion rate in plagioclase, its composition reflects the conditions of crystallization or reprecipitation. Plagioclase was therefore selected from the groundmass in the vicinity of garnets (Holdaway, 2001), but away from any embayment in garnet (in rare cases where such embayments are present) to avoid plagioclase possibly formed by the retrograde net transfer reaction (7). Moreover, plagioclase rims were preferred over cores to avoid plagioclase that would have formed on the prograde path at lower temperatures than that corresponding with the re-equilibrated garnet core composition. Although great precautions were taken in the selection of minerals, it is difficult to ascertain that the calculated P-T truly represent the highest P-T conditions attained by the rocks. Results should therefore be considered minimum estimates of the peak P-T conditions.

The strategy adopted for the amphibolite sample RS011-082B is different and is described in detail along with the description of the textures to facilitate comprehension.

### 5.3. Results

A summary of the chemical compositions and the calculated P-T results is presented in table 1, garnet zoning profiles are presented on Fig. 6, and the complete chemical composition spreadsheets for the analyzed minerals is provided as supplementary data table 1. The following section outlines the major compositional variations observed in the minerals and presents the thermobarometric results obtained from the three different domains.

#### 5.3.1. Interior of the Mékinac-Taureau domain in the footwall of the TSZ (RS12-021)

Zoning profiles of euhedral garnet porphyroblasts are typically flat (Fig. 6A) and show little inter-crystal variation. Biotite shows variation in chemical composition based on their relationship with garnet. Biotite in contact with garnet typically has low Fe/(Fe+Mg) values compared to isolated biotite (0.31-0.33 vs. 0.36-0.39, respectively). Plagioclase is abundant and commonly has sharp, straight contacts with garnet. Its composition is relatively homogenous (An<sub>43</sub>-An<sub>46</sub>). Calculated pressures and temperatures range from 1050 to 1120 MPa and from 819 to 849 °C, respectively.



### 5.3.2. External zone of the Mékinac-Taureau domain near the TSZ (RS11-058 and RS12-015A)

Garnet from these samples is not strongly resorbed and locally preserve pristine crystalline faces. Garnet zoning profiles of  $\text{Fe}/(\text{Fe}+\text{Mg})$  are generally flat or increases slightly from the core towards the rim, (maximum variation ( $\Delta$ )  $<0.08$ ) (Fig. 6B-C). Garnet zoning profiles of  $X_{\text{sps}}$  and  $X_{\text{grs}}$  are flat throughout. Garnet show little inter-crystal variations, with the exception of rare smaller grains ( $<1$  mm) that have abnormally high  $\text{Fe}/(\text{Fe}+\text{Mg})$  values that were thus excluded from calculations. Biotite in contact with garnet typically has low  $\text{Fe}/(\text{Fe}+\text{Mg})$  values compared to isolated biotite (0.36-0.37 vs. 0.40-0.44 and 0.26-0.34 vs. 0.36 vs 0.44 for samples RS11-058 and RS11-015A, respectively). Sample RS11-058 contains relatively homogeneous plagioclase ( $\text{An}_{37}\text{-An}_{41}$ ), but sample RS12-15A contains rare plagioclase (only five analyses) of variable composition ( $\text{An}_8\text{-An}_{20}$ ) that occurs as anhedral masses within or next to K-feldspar. In the latter sample, the large variation of composition, the small number of analyses, and the high probability that Ca-poor plagioclase is the result of exsolution or secondary precipitation prevented a confident selection of an appropriate plagioclase composition for geothermobarometric calculations. In sample RS11-058, calculated pressure ranges from 780 to 790 MPa and temperature was determined at 780 °C. Because of the lack of satisfactory plagioclase analyses in sample RS12-015A, no pressure determinations were attempted. However, a temperature range of 740-780 °C was obtained, assuming a conservative pressure range of 600-1100 MPa.

### 5.3.3. Shawinigan domain above the TSZ (RS12-027B and RS11-105)

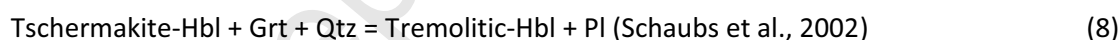
Garnet in sample RS12-27B is well preserved, whereas embayments filled with large unoriented biotite are locally present at the margins of garnet in sample RS11-105.  $\text{Fe}/(\text{Fe}+\text{Mg})$  zoning profiles of all garnet from this domain are flat in the cores and increase in the rims ( $<0.07$ , Fig. 6D-G).  $X_{\text{grs}}$  profiles are typically flat, but a gradual decrease in  $X_{\text{grs}}$  ( $\Delta <0.02$ ) may be observed towards the rim of some garnets. In sample RS12-027B,  $X_{\text{sps}}$  is constant from core to rim, whereas systematic increases of Mn ( $<0.01 X_{\text{sps}}$ ) are observed on garnet rims of sample RS11-105. Sample RS11-105 also contains three populations of garnet, occurring randomly in the thin section, that have similar composition profiles but different absolute concentrations of Fe, Mg and Ca. Their morphology is also different: type 1 is characterized by abundant ilmenite inclusions in the core with an inclusion-poor rim (Fig. 5C); type 2 is characterized by abundant quartz inclusions in the core and inclusion-poor rim (Fig. 5D); whereas type 3 consists of inclusion-poor garnet (Fig. 5E).

Biotite in contact with garnet has systematically lower Fe/(Fe+Mg) compared to armoured biotite (0.40-0.47 vs. 0.47-0.48 and 0.51-0.54 vs 0.53-0.56 for samples RS12-027B and RS11-105, respectively). In sample RS11-105, no systematic variation of the Fe/(Fe+Mg) value in biotite with position was observed that could be related to the garnet type. Plagioclase is abundant in both samples and commonly found in stable contact with garnet. Its composition varies between An<sub>32</sub> and An<sub>38</sub> in sample RS12-027B whereas sample RS11-105 contains homogeneous plagioclase (An<sub>21</sub>-An<sub>22</sub>). Ca-poor plagioclase (An<sub>2</sub> to An<sub>15</sub>) in sample RS12-027B, occurring as patches in K-feldspar and interpreted as the result of exsolution or secondary precipitation, was not used for thermobarometric calculations.

Sample RS12-27B yielded pressures and temperature of 740-790 MPa and 780 °C. In sample RS11-105, calculated pressures and temperatures for type 1 garnet range from 720 to 860 MPa and from 730 to 750 °C, respectively, whereas both types 2 and 3 garnets registered lower P-T conditions of 620-650 MPa and 700-710 °C.

#### 5.3.4. Eastern TSZ (RS11-082B)

This amphibolite contains sigmoid-shaped coronas of plagioclase and minor hornblende surrounding garnet (Fig. 5F), in a groundmass of Hbl + Pl + Qtz + Mag + Ilm + Ttn. It also shows plagioclase-rich patches similar in size to garnet crystals and surrounded by the same groundmass, that are interpreted as garnet pseudomorphs formed from the retrograde decompression reaction:



The sigmoidal shape of the reaction rims suggests that they are pre- to syn-kinematic with respect to top-down-to-the-ESE movement. Retrograde conditions obtained with this sample therefore provides P-T constraints corresponding to shearing along the eastern TSZ.

The chemical compositions of minerals in this sample supports this interpretation because they systematically vary according to their textural locations. Fe/(Fe+Mg) and X<sub>sps</sub> profiles in garnet are either flat or progressively decreases from core to inner rim ( $\Delta < 0.05$  and 0.04, respectively; Fig. 6H). The largest garnet grains present evidence of a prograde P-T path (Fig. 6H) with a gradual increase in X<sub>grs</sub> from core to inner rim ( $\Delta < 0.09$ ) followed by decompression evidenced by a sharp decrease in X<sub>grs</sub> towards the outer rim ( $\Delta < 0.13$ ). Two populations of hornblende are recognized. The first occurs as large (1000-3000  $\mu\text{m}$ ) crystals in in the groundmass and is characterized by higher Fe/(Fe+Mg) values (0.43-

0.45) compared to the second population composed of small (100-400 $\mu$ m) in the coronas surrounding the garnet ( $\text{Fe}/(\text{Fe}+\text{Mg})=0.40-0.44$ ). Plagioclase from the groundmass yield values of  $\text{An}_{40}$  to  $\text{An}_{51}$  that are clearly distinctive from that in the coronas, which yield values of  $\text{An}_{49}$  to  $\text{An}_{58}$ . These patterns suggest that thermobarometry could provide good estimate on peak and retrograde conditions.

Our interpretation that the disequilibrium coronitic texture linked with chemical variation in minerals provide information about the peak and retrograde history of the rock requires two conditions. First, parts of garnet, plagioclase and hornblende must have been in chemical equilibrium at the scale of the thin-section when the rock was at peak and at the end of the retrograde path. Second, chemical compositions that prevailed at the peak were preserved in parts of several minerals despite subsequent diffusion and recrystallization that took place afterward. If these two conditions are met in our sample, then every P-T calculated from any garnet-plagioclase-hornblende compositions interpreted to have been in equilibrium at peak or at the end of the retrograde path should yield the same values within analytical and reasonable geological errors. We tested this by using the software TC\_Comb (Dolivo-Dobrovolsky, 2013, <http://www.dimadd.ru/en>) that allows rapid P-T calculations by the average PT method (Holland and Powell, 1994) for all possible permutations of a set of mineral compositions. As a set interpreted to reflect peak mineral compositions, we selected 17 analyses from the core of four garnet grains showing minimal evidence of diffusion (i.e. flat for at least two successive points), the six hornblende analyses located in the matrix, and the four plagioclase analyses located in the groundmass near the selected garnet grains. Calculations of P-T for all permutations of these analyses resulted in a well clustered cloud of correlated points yielding mean temperature and pressure of  $880 \pm 80^\circ\text{C}$  and  $990 \pm 120$  MPa, respectively. To calculate retrograde conditions, we selected five analyses from the rim of five garnet grains surrounded by a plagioclase + hornblende coronae, as well as six hornblende and 22 plagioclase grains located in these coronas. Calculations of P-T for all permutations of these analyses resulted in a well clustered cloud of correlated points yielding mean temperature and pressure of  $720 \pm 30^\circ\text{C}$  and  $650 \pm 50$  MPa, respectively. The uncertainties are  $2\sigma$  and do not reflect uncertainties associated with the mineral database. The difference between these mean values are highly significant ( $p < 0.0001$ ) yielding  $162^\circ\text{C}$  with a 95% confidence interval of  $157-166^\circ\text{C}$  and 340 MPa with a 95% confidence interval of 330-350 MPa. These results clearly demonstrate that minerals in amphibolite sample RS11-082B reached chemical equilibrium at peak and at the end of the retrograde path and that the two P-T conditions are clearly distinct.

#### 5.4. Interpretation of thermobarometry results

The chemical compositions of analyzed garnet and biotite reveal important information about the metamorphic history of the metapelites from the Mauricie area. First, completely flat  $\text{Fe}/(\text{Fe}+\text{Mg})$ ,  $X_{\text{grs}}$  and  $X_{\text{sps}}$  zoning profiles of most garnets from the interior of the Mékinac-Taureau domain suggest complete intra-crystalline diffusion of Fe, Mg, Ca and Mn in garnet during peak metamorphism. Since biotite in contact with garnet has a lower  $\text{Fe}/(\text{Fe}+\text{Mg})$  value compared to armoured biotite, the exchange reaction (1) probably occurred during retrograde metamorphism, but the expected opposite pattern is not present in adjacent garnet, probably because the transects were located away from zones of contact with biotite. Most importantly, garnet in sample RS11-021 is euhedral (Fig. 5B) and does not show a variation in  $X_{\text{sps}}$ , which suggests that it did not start to break down via the retrograde net transfer reaction (7).

Pressure and temperature calculated with compositional plateaus in garnet core, armoured biotite and matrix plagioclase are therefore interpreted as the metamorphic peak conditions of the Mékinac-Taureau domain. The calculated conditions of  $\sim 1075$  MPa and  $\sim 825$  °C lie in the kyanite stability-field and could suggest underestimation of the temperature, but they are nonetheless within error of the sillimanite stability-field, and hence in agreement with petrographic observations considering uncertainties. The temperature measured in this study is in agreement with previous results of  $\geq 800$  °C by (Corrigan, 1995; Herd et al., 1986). However, the pressure estimate of 1075 MPa is above the previous results of 800-900 MPa (Corrigan, 1995; Herd et al., 1986).

In the external zone of the Mékinac-Taureau domain, garnet cores in metapelite have essentially flat zoning profiles in  $\text{Fe}/(\text{Fe}+\text{Mg})$ ,  $X_{\text{grs}}$  and  $X_{\text{sps}}$ , suggesting complete intra-crystalline diffusion of Fe, Mg, Ca and Mn in garnet during peak metamorphism. However, garnet crystals show a slight increase in  $\text{Fe}/(\text{Fe}+\text{Mg})$  toward their rims ( $\Delta < 0.08$ ). This is the result of limited diffusion by the retrograde exchange reaction (1). The systematic decrease in  $\text{Fe}/(\text{Fe}+\text{Mg})$  value of biotite in contact with garnet, as compared with armoured biotite, supports such an interpretation. The lack of  $X_{\text{sps}}$  increase at the rim suggests that the garnet consuming net transfer reaction (7) did not operate. The pressure of 790 MPa and temperature of  $\sim 775$  °C calculated with compositional plateaus from the garnet core, armoured biotite and matrix plagioclase are therefore interpreted as the prevailing conditions during high grade Grt-Bt re-equilibration in the external zone of the Mékinac-Taureau domain. Furthermore, Grt and Bt were only

affected to a limited degree by the retrograde exchange reaction (1) and chemical compositions used for calculations were selected to avoid the effects of this reaction. A metamorphic temperature estimate of  $\sim 770^\circ\text{C}$  in the southeastern margin of the Mékinac-Taureau domain has been previously provided by Lévesque (1995), which is consistent with data presented above. In any case, these results are lower than metamorphic peak conditions obtained for the interior of the Mékinac-Taureau domain.

The amphibolite RS11-082B collected at the eastern TSZ indicates that similar P-T conditions of  $\sim 990\text{ MPa}$  and  $\sim 880^\circ\text{C}$  prevailed during the metamorphic peak throughout the Mékinac-Taureau domain. As shown on Fig. 7, peak and retrograde P-T values are equivalent to those yielded by the metapelites from the interior and the margin of the Mékinac-Taureau domain. The statistical analysis further demonstrates that the difference between the mean peak and retrograde P-T conditions are significant. Moreover, the reaction rims around garnet in the amphibolite were deformed during top-down-to-the-ESE shearing along the eastern TSZ and must have formed prior to or during that shearing. This implies that the eastern TSZ was formed under P-T conditions  $\leq 600\text{--}700\text{ MPa}$  and  $\leq 675\text{--}775^\circ\text{C}$ , respectively.

In the Shawinigan domain, garnet cores in metapelite have essentially flat zoning profiles  $\text{Fe}/(\text{Fe}+\text{Mg})$ ,  $X_{\text{grs}}$  and  $X_{\text{sps}}$ , suggesting complete intra-crystalline diffusion of Fe, Mg, Ca and Mn in garnet during peak metamorphism. However, garnet crystals show a slight increase  $\text{Fe}/(\text{Fe}+\text{Mg})$  toward their rims ( $\Delta < 0.07$ ). Sample RS11-105 contains garnet that has a small  $X_{\text{sps}}$  increase at the rim ( $\Delta < 0.02$ ), which probably resulted from net transfer reaction (7). Such reactions theoretically increase the  $\text{Fe}/(\text{Fe}+\text{Mg})$  value of biotite in contact with garnet, but in our sample,  $\text{Fe}/(\text{Fe}+\text{Mg})$  values are lower in biotite in contact with garnet as compared to armoured biotite. This suggests that the effect of net transfer reaction (7) was overwhelmed by the effect of exchange reaction (1), which decreases the  $\text{Fe}/(\text{Fe}+\text{Mg})$  value of biotite. Although the retrograde exchange and net transfer reactions (1) and (7) affected the composition of the rim of garnet, the large compositional plateau in the core indicates a complete Grt-Bt re-equilibration at high temperature. P-T values yielded by this sample are dispersed along an array (Fig. 7) with types 2-3 garnets lying on the lower grade side and type 1 garnet on the higher grade side. This may suggest two episodes of garnet growth. Chemical plateaus in type 1 garnets imply complete intra-crystalline diffusion at higher grade than conditions recorded by types 2-3. Considering that type 2 garnets are equivalent in size to type 1 and that type 3 garnets are approximately half the size of type 1

garnet, prograde conditions cannot be preserved in types 2-3 garnets. An alternative hypothesis would be that types 2-3 garnets grew during decompression and cooling, but this would require an unexplained thermal spike during the retrograde path. Molar isopleths of garnet in metapelites (e.g. Storm and Spear, 2005) have steep slopes on P-T diagrams for the considered P-T conditions (i.e. 625-650 MPa and 700 °C). Therefore, temperature must increase to produce new garnet. It may also be possible that abundant ilmenite inclusions in type 1 garnet induce a Fe/(Fe+Mg) decrease in garnet that results in over-estimation of metamorphic conditions. Pressure and temperature calculated with compositional plateaus from garnet core of samples RS12-027B and RS11-115 along with and armoured biotite and matrix plagioclase are interpreted as the metamorphic peak conditions of the Shawinigan domain at ~625-850 MPa and ~700-775 °C. Such metamorphic conditions are consistent, within error, with data from Lévesque (1995) (725-800 °C at 720-880MPa).

In summary, the necessary precautions in the selection of minerals were taken and we carefully interpreted the results to provide meaningful P-T values for high grade rocks. The non-existent to limited effects of the retrograde net transfer reaction (7), allowed the preservation of large chemical plateaus in the cores of garnets. Peak metamorphism in the Mékinac-Taureau domain attained P-T conditions of 1000-1100 MPa and 820-880 °C, whereas retrograde conditions varying from 800 to 650 MPa and from 775 to 675 °C were recorded in its upper structural levels. The Shawinigan domain records P-T conditions varying from 850 to 625 MPa and from 775 to 700 °C. The decreasing P-T trend from the Mékinac-Taureau domain to the Shawinigan domain described in this study is therefore significant.

## 6. U-Pb geochronology

### 6.1. Pegmatite samples description and setting

#### 6.1.1. Sample RS11-098

In order to constrain the timing of deformation along the eastern TSZ, a pegmatite intrusion synchronous with normal shearing (RS11-098) was sampled at the St-Tite gravel pit (Fig. 8A). This pegmatite has a granitic composition (Qtz + Kfs + Pl + Bt + Chl (late) + Zrn + Mnz) and forms a 3-m wide body, from which the analyzed sample was collected, surrounded by abundant dykelets, extending away from it. The pegmatite cross-cuts the  $S_{n+1}$  foliation in the host gneiss ( $S_{n+1} \approx 330/32$ ), but locally shows a weakly-developed internal foliation parallel to  $S_{n+1}$ . Contacts with the host gneiss are sharp and the

composition of the pegmatite is homogeneous, suggesting they are dilation dykes (in the sense of Goodspeed, 1940). Above the main body of pegmatite, a series of foliated dykelets is clearly transposed parallel to  $S_{n+1}$  whereas the foliation in the hosting gneiss forms S-shaped planes. Planar fabrics defined by both the pegmatite dykelets and the host rock foliation are interpreted as similar to a C-S structure indicating top-down-to-the-ESE shearing (Fig. 8B). The transposition of S planes during shearing was probably interrupted by the emplacement of the dykelets, which then accommodated further strain. To the right end of the pegmatite body, a 20 cm-thick dyke dips ESE and cuts across  $S_{n+1}$  at an angle of  $\sim 40^\circ$ . Inasmuch as this orientation is perpendicular to the minimum shortening direction under top-down-to-the-ESE shearing, this dyke, which resemble extensional fault-propagation fold and associated dilation dike (Schwerdtner et al. 2014), is interpreted to have been emplaced in a fracture conjugate to the shear plane (e.g. Davidson et al., 1994). At the margins of that dyke,  $S_{n+1}$  is dragged downward on the NW side and upward on the SE side, which is also consistent with top-down-to-the-ESE (Fig. 8A). We therefore consider that the isotopic dating of pegmatite crystallization provides an age constraint for the normal-sense shearing deformation observed on the eastern TSZ.

#### 6.1.2. Sample RS12-040

Another granitic pegmatite (RS12-040) was sampled at an outcrop located approximately 2 km structurally below the eastern TSZ. This outcrop is composed of strongly migmatized and folded, felsic to mafic orthogneiss. Leucosome material contains orthopyroxene and is commonly trapped within the hinges of recumbent folds of undetermined vergence, indicating that partial melting was mostly contemporaneous with peak metamorphism and deformation. Moreover, some pockets of leucosome locally cut across the foliation, suggesting that partial melting outlasted deformation and possibly occurred after metamorphic peak. Because this outcrop does not show evidence of shearing typical of the eastern TSZ, deformation there is attributed to the older event associated with the development of foliation  $S_n$ . The sampled pegmatite is made up of Qtz + Kfs (perthitic) + Pl + Bt + Chl (late) + Zr + Mnz and opx-bearing leucosome in the host gneiss commonly merges into the pegmatite without clear cross-cutting relationships. Contact between the pegmatite dyke and the host gneiss melanosome is sharp and rectiplanar, suggesting that the pegmatite dyke is a dilation dyke (Goodspeed, 1940). Its crystallization age therefore provides a minimum age for the deformational episode related to crustal thickening and associated peak metamorphism.

## 6.2. Analytical methods

Zircon grains were separated from rocks using standard techniques. Zircon was mounted in epoxy, polished until the centers of the grains were exposed, and imaged with cathodoluminescence (CL). Zircon was analyzed by Laser Ablation Inductively Coupled Plasma Mass Spectrometry (LA-ICPMS) using a ThermoElectron X-Series II quadrupole ICPMS and New Wave Research UP-213 Nd:YAG UV (213 nm) laser ablation system at Boise State University (Idaho, USA). In-house analytical protocols, standard materials, and data reduction software were used for acquisition and calibration of U-Pb dates and a series of selected high field strength (HFSE) and rare earth elements (REE). Zircon grains were ablated with a laser spot of 25 and 30  $\mu\text{m}$  wide. Additional details concerning analytical methods are available in the supplementary data repository.

For groups of analyses that were collectively interpreted as a weighted mean date (i.e., igneous zircon analyses), a weighted mean date was first calculated with Isoplot 3.0 (Ludwig, 2003) using errors on individual dates that do not include a standard calibration uncertainty, and then a standard calibration uncertainty was propagated into the error on the weighted mean date. Age interpretations are based on weighted mean  $^{207}\text{Pb}/^{206}\text{Pb}$  dates, which are more precise than U/Pb dates upon propagation of the standard calibration uncertainties and not affected by recent Pb loss. Analyses that are >15% discordant are interpreted as being from domains that lost Pb and were not considered. A few analyses with <15% discordance were not included in the weighted mean calculations because they are not equivalent with the other dates, most likely due to small amounts of Pb loss ( $^{206}\text{Pb}/^{238}\text{U}$  dates) or common Pb ( $^{207}\text{Pb}/^{206}\text{Pb}$  dates). Errors on the  $^{207}\text{Pb}/^{206}\text{Pb}$  and  $^{206}\text{Pb}/^{238}\text{U}$  dates from individual analyses are given at  $2\sigma$ , as are the errors on the weighted mean dates.

## 6.3. Results

### 6.3.1. Pegmatite sample RS11-098

Zircon was classified into four compositional groups according to trace element concentrations. Some differences are also apparent in their morphology and zoning patterns in cathodoluminescence (CL) images (Fig. 9A). Trace element contents are presented below in the following format: (min-max values; average value). Complete chemical composition data and Concordia diagrams are presented in supplementary data table 2 and Fig. S1.



Group 1 zircon is composed of homogeneous to oscillatory-zoned, CL dark, subequant grains (Fig 9A), characterized by high U and Th contents (210-420; 306 and 110-330; 201 ppm; Fig 10A) and low Th/U values (0.5-0.8; 0.7). It has medium Y (480-1300; 829 ppm), Nb (4-8; 5 ppm), Hf (9940-11530; 10783 ppm), middle rare earth elements (MREE: Sm-Gd) and heavy rare earth elements (HREE: Tb-Lu) contents.

Group 2 zircon is composed of CL paler grains that are frequently sector or patchy zoned. It commonly forms individual grains and/or secondary rims of overgrowth on Group 1 (Fig 9A). It is characterized by low to medium U content (80-210; 133 ppm; Fig 10A), low Th content (60-190; 101 ppm; Fig 10A) and low Th/U value similar to group 1 (0.5-0.9; 0.8). It has relatively low Y (360-970; 591 ppm), Nb (2-5; 3 ppm), MREE, HREE contents and relatively high Hf content (9200-13410; 10968 ppm).

Group 3 zircon is composed of CL pale oscillatory and patchy zoned zircon. It usually forms individual grains, but one occurrence shows Group 3 zircon rim overgrowing a Group 1 zircon core (Fig 9A). Group 3 is characterized by low U content, (50-130; 103 ppm; Fig 10A), medium Th content (70-210; 157 ppm; Fig 10A) and relatively high Th/U value (1.1-1.8; 1.5). It has relatively high Y (750-1450; 1198 ppm), Nb (2-7; 6 ppm), MREE and HREE contents and relatively low Hf content (7820-10930; 9407 ppm).

Group 4 zircon is composed of homogeneous to patchy zoned CL dark cores (Fig 9A). It has low to very high U and Th content (100-650; 387 and 90-510; 300; Fig 10A) and medium Th/U values (0.5-1.0; 0.8). It has relatively high Y (940-1920; 1491 ppm) and Nb (1-9; 6 ppm) contents, very high MREE (Sm-Gd) and HREE (Tb-Lu) contents and relatively low Hf content (7210-11780; 9855 ppm).

Differences and similarities in the chemical composition of Groups 1-4 are well illustrated by a series of selected compositional variation diagrams (Fig. 10). The distinction between zircon groups is particularly obvious in the Th vs. U diagram (Fig. 10A), in which each group shows a distinctive compositional trend that reflects variations in the Th/U value. Other diagrams such as Lu/Hf vs. Th/Y, and Th/Y vs. Y/Hf (Fig. 10B-C) also show clear differences between the four groups. Groups 1 and 2 typically have overlapping chemical compositions, whereas Group 3 is clearly distinguishable, as shown by the Nb/U vs. Th/U diagram (Fig. 10D). Group 4 comprises zircon cores of various chemical compositions that generally lie off the chemical compositional field of Groups 1-3 in some diagrams.

The temperature of crystallization of the analyzed zircon grains was calculated based on the Ti-in-

zircon thermometer, developed by Watson et al. (2006), using the more recent calibration of Ferry and Watson (2007) and the pressure dependence of Ferriss et al. (2008). For Groups 1-3,  $a\text{TiO}_2=0.8$  and  $P=700$  MPa were used to correct the temperature calculations, whereas the same  $a\text{TiO}_2$  without any pressure correction (i.e.  $P=1000$  MPa) were used for Group 4. All temperatures of crystallization are subject to an uncertainty of  $\pm 30$  °C comprising uncertainties on the Ti content measurement, on the calibration error of the thermometer equation, on the estimated value of  $a\text{TiO}_2$  and on the estimated pressure during crystallization, all added in quadrature. Additional details on the calculation of the uncertainty and the choice of correction factors are available in the supplementary data repository. The average temperature of crystallization of Group 1 is 691 °C; Group 2 is 703 °C and Group 3 is 707 °C. Group 4 zircon crystallized at temperature varying from 716 to 794 °C.

All interpretations are based on  $^{207}\text{Pb}/^{206}\text{Pb}$  dates (Fig. 11A-C) because they are more precise upon propagation of calibration errors and not affected by recent Pb loss.  $^{206}\text{Pb}/^{238}\text{U}$  dates are nonetheless presented here for comparison purposes, but were not used in interpretations. Weighted mean  $^{207}\text{Pb}/^{206}\text{Pb}$  and  $^{206}\text{Pb}/^{238}\text{U}$  dates obtained from Groups 1-3 are equivalent whereas they are older in Group 4. Group 1 yielded a  $^{207}\text{Pb}/^{206}\text{Pb}$  date of  $1064 \pm 15$  Ma (mean square weighted deviation (MSWD)=1.3, probability of fit (PF)=0.16, number of analyses (n)=22) and a  $^{206}\text{Pb}/^{238}\text{U}$  date of  $1058 \pm 27$  Ma (MSWD=1.1, PF=0.32, n=21). Group 2 yielded a  $^{207}\text{Pb}/^{206}\text{Pb}$  date of  $1058 \pm 16$  Ma (MSWD=1.1, PF=0.34, n=28) and a  $^{206}\text{Pb}/^{238}\text{U}$  date of  $1042 \pm 26$  Ma (MSWD=0.9, PF=0.55, n=25). Group 3 yielded a  $^{207}\text{Pb}/^{206}\text{Pb}$  date of  $1063 \pm 17$  Ma (MSWD=1.4, PF=0.08, n=31) and a  $^{206}\text{Pb}/^{238}\text{U}$  date of  $1047 \pm 26$  Ma (MSWD=1.0, PF=0.41, n=34). Group 4 yielded  $^{207}\text{Pb}/^{206}\text{Pb}$  dates of  $1459 \pm 50$  to  $1052 \pm 53$  Ma and  $^{206}\text{Pb}/^{238}\text{U}$  dates of  $1421 \pm 60$  to  $1032 \pm 58$  Ma.

### 6.3.2. Pegmatite sample RS12-040

The chemical composition, morphology, zoning patterns in CL images and age of zircon from sample RS12-040 do not define distinct groups. These analyses are consequently treated as a unique group. Dark xenocrystic cores were easily distinguished and avoided during analysis. Trace element contents are presented in the following format: (min-max values; average value) and the complete chemical composition data and Concordia diagram are presented in supplementary data table 2 and Fig. S1. Zircon grains are generally prismatic and have an aspect ratio varying from 1:1 to 1:5. They are commonly oscillatory zoned and dark in CL (Fig. 9B). They are characterized by medium to high U and Th

contents (90-340; 166 and 40-570; 252) and high Th/U values (0.1-2.9; 1.52). They have high Y and Nb content (540-2790; 1148 and 3-8; 6), variable Hf content (8230-15060; 10362), medium MREE and relatively high HREE (Tb-Lu) contents. Their temperature of crystallization has been estimated at  $755 \pm 30$  °C with  $a\text{TiO}_2=0.8$  and  $P=1000$  MPa.

Weighted mean  $^{207}\text{Pb}/^{206}\text{Pb}$  and  $^{206}\text{Pb}/^{238}\text{U}$  dates from sample RS12-040 are equivalent. It yielded a  $^{207}\text{Pb}/^{206}\text{Pb}$  date of  $1082 \pm 20$  Ma (Fig. 11D; MSWD=1.4, PF = 0.06, n=35) and a  $^{206}\text{Pb}/^{238}\text{U}$  date of  $1055 \pm 34$  Ma (MSWD=1.3, PF=0.11, n=39).

#### 6.4. Interpretation of zircon chemical composition and U-Pb dates

Relatively large errors on U-Pb dates yielded by the LA-ICP-MS method preclude a clear distinction between Groups 1-3 zircons of the pegmatite sample RS11-098. More precise TIMS dating is needed to precisely determine age differences, if any. However, petrographical relationships suggest that Group 1 zircon grains are the oldest since they are commonly overgrown by Group 2 and rarely by Group 3 (Fig. 9A). Given their homogeneous chemical composition and the lack of sector zoning or zonation perturbation, Group 1 zircon grains are interpreted as primary igneous zircons that formed during the crystallization of the pegmatite. The great compositional similarity between Groups 1 and 2 zircons suggests that Group 2 formed by recrystallization and/or dissolution and re-precipitation of Group 1. Such an interpretation is supported by the constant depletion in non-essential structural constituent cations such as U, Th, Y, Nb and REE, which are commonly removed in fluid-altered zircon, of Group 2 as compared to Group 1 (Hoskin and Black, 2000; Hoskin and Schaltegger, 2003). Furthermore, the small enrichment in Hf content of Group 2 zircon compared to Group 1 is also characteristic of recrystallization of a pre-existing zircon population (Pan, 1997). Finally, the patchy and sector zonation common in Group 2 is considered as typical of metamorphic zircon or igneous zircon perturbed by late-magmatic processes (Corfu et al., 2003).

Group 3 zircon has a distinct chemical composition, suggesting that it possibly originated from a distinct fluid phase. Rare overgrowing of Group 1 zircon grains indicates that Group 3 zircon is younger, but no physical relationship were observed between Groups 2 and 3 (Fig. 9A). Group 3 zircon comprises mostly patchy zoned crystals that probably grew in solid state, but minor oscillatory zoned zircon grains suggest that some may have grown in the presence of a fluid phase. Group 3 zircon is therefore interpreted as metamorphic, but derived from a different source than that of Group 2. Scarcity of Group

3 zircon overgrowing Groups 1-2 zircons would be explained if Group 3 zircon only formed in discrete domains related to fluid infiltration following the crystallization of the pegmatite. However, further in-situ work on new samples is needed to test this hypothesis since the crushing process destroyed evidence of any such domains, if present.

Group 4 is composed of zircon cores of various chemical compositions that do not fit with Group 1-3 chemical composition. Group 4 also typically yields older U-Pb dates and is therefore interpreted as being xenocrystic (inherited).

Temperatures of crystallization of Groups 1-3 (691 °C, 703 °C and 707 °C, respectively) are equivalent within the  $\pm 30$  °C uncertainty. Since the pegmatite was emplaced during the exhumation of the hosting units, it would be expected to see a temperature decrease from the oldest to the youngest group of zircons. However, such a decrease is not resolvable with the present data. A 14 °C increase is even observed from group 1 to group 3. A pressure decrease between Group 1 and Group 3 crystallization would elegantly explain this apparent increase in temperature, because pressure decrease leads to overestimation of the temperature calculated with the Ti-in-zircon thermometer (Ferris et al., 2008; Ferry and Watson, 2007). However, the large uncertainties on many other parameters (especially  $a_{\text{TiO}_2}$ ) impede confident interpretation of temperature variations between zircon groups from sample RS11-098. Nonetheless, temperatures calculated for the crystallization of Groups 1-3 zircons ( $691\text{--}707 \pm 30$  °C) are equivalent, within error, to temperatures of retrograde metamorphism registered by the amphibolite and the metapelites of the upper structural levels of the Mékinac-Taureau domain ( $675\text{--}775 \pm 50$  °C; section 5.3). Temperatures of zircon crystallization thus support the emplacement of the pegmatite during retrograde metamorphism and exhumation of this domain. The crystallization of this syn-kinematic pegmatite at  $1064 \pm 15$  Ma (Group 1,  $^{207}\text{Pb}/^{206}\text{Pb}$ ) therefore provides a time constrain on the top-down-to-the-ESE shearing along the eastern TSZ.

Zircon from sample RS12-040 is interpreted as igneous because of their prismatic shape, oscillatory zoning and high trace elements content (e.g. U, Th, Y, Nb, HREE) (Corfu et al., 2003). The temperature of crystallization of pegmatite RS12-040 ( $755 \pm 30$  °C) is higher as compared to pegmatite RS11-098 ( $691 \pm 30$  °C). This is consistent with the emplacement of pegmatite RS12-040 after peak metamorphic conditions of  $820\text{--}880$  °C  $\pm 50$  °C, but before the emplacement of pegmatite RS11-098, which was emplaced during cooling and extension along the eastern TSZ at  $1064 \pm 15$  Ma. The age of

crystallization of the pegmatite RS12-040 ( $1082 \pm 20$  Ma,  $^{207}\text{Pb}/^{206}\text{Pb}$ ) implies a minimum age constraint for deformation and metamorphism related to thrusting and crustal thickening in the Mékinac-Taureau domain. That result is moreover consistent with data of Corrigan and van Breemen (1997) who suggested a lower age limit of  $1087 \pm 2$  Ma for the thrusting in the adjacent Shawinigan domain.

## 7. $^{40}\text{Ar}/^{39}\text{Ar}$ geochronology

### 7.1. Analytical methods

Amphibole and biotite single grains from the the Mékinac-Taureau domain were dated by the  $^{40}\text{Ar}/^{39}\text{Ar}$  method (Géosciences Rennes, UMR CNRS 6118) using a  $\text{CO}_2$  laser probe. The experimental procedure has been described by Ruffet et al. (1991, 1995) and Cathelineau et al. (2012). All plateau and pseudo-plateau ages are displayed at the  $2\sigma$  level. Analytical data, parameters used for calculations (isotopic ratios measured on K, Ca and Cl pure salts; mass discrimination; atmospheric argon ratios; J parameter; decay constant, etc.) and reference sources are available in the supplementary data repository.

Isotopic mineral ages are interpreted to record cooling below the closure temperature ( $T_c$ ). Closure temperatures for amphibole are difficult to estimate because amphibole diffusivity is influenced by the cooling rate, the size of diffusion domains and ionic porosity (Dahl, 1996; Fortier and Giletti, 1989). On the basis of natural hornblende compositions measured by various authors (i.e. Leake, 1978; Robinson et al., 1982), Dahl (1996) suggested a  $T_c$  range of 480–560 °C, calculated for an effective diffusion radius of 80  $\mu\text{m}$  and a cooling rate of 10 °C/Ma. Harrison (1981) calculated closure temperatures between 500 °C and 580 °C for an effective diffusion radius of 80  $\mu\text{m}$  and cooling rates in the range of 10 to 500 °C/Ma. The closure temperature was revised to 550–650 °C by Villa (1998) using Dahl's (1996) experiments suggesting that, depending on its lattice characteristics, hornblende may form a closed system for Ar diffusion at temperatures as high as 580 °C under cooling rates of 0.7 K/Ma (Villa et al., 1996). Recent re-assessments of the closure temperature for biotite suggest that it may be as high as 450 °C (e.g. Allaz, 2008; Allaz et al., 2011; Villa and Puxeddu, 1994), 150 °C higher than the commonly accepted temperature of 300 °C (ex: Dodson, 1973; Harrison et al., 1985). In this study, we will consequently use a  $T_c$  range value of 550–600 °C and around 450 °C for Ca-amphibole and biotite, respectively.

## 7.2. Results

Six samples containing coarse amphibole and/or biotite were collected in the Mékinac-Taureau and the Shawinigan domains to investigate the cooling history of the area through  $^{40}\text{Ar}/^{39}\text{Ar}$  geochronology (See Fig. 2 for locations and supplementary data table 3 for complete results). With one exception, all samples yielded undisturbed plateau ages for both amphibole and biotite (Fig. 12, Table 2). Samples RS11-002 and RS11-115 come from two amphibole- and biotite-rich mafic layers transposed into parallelism with the hosting orthogneiss foliation ( $S_n$ ) in the interior of the Mékinac-Taureau domain, and located, respectively, ~11 and ~9 km structurally below the eastern TSZ. They yielded amphibole plateau ages of  $998.6 \pm 7.4$  Ma and  $1010.0 \pm 7.4$  Ma, respectively (Fig. 12A and 12B). Biotite plateau ages of  $923.2 \pm 7.0$  Ma and  $969.8 \pm 7.2$  Ma, respectively, were also obtained from these samples (Fig. 12A and 11B). Sample RS11-015 comes from a metapelite layer located ~3 km below the TSZ and contains biotite but not amphibole. The biotite spectrum defines a plateau at  $926.1 \pm 7.0$  Ma (Fig. 12C). Sample RS11-089 is a biotite-free amphibolite layer located within the eastern TSZ, on the Mékinac-Taureau domain side, that yielded an amphibole plateau age of  $1031.6 \pm 7.6$  Ma (Fig. 12D). Finally, two samples were collected in the Shawinigan domain: RS11-113 is a biotite and amphibole bearing intermediate orthogneiss whereas RS11-105 is an amphibole-free metapelite. These samples are respectively located ~1 km and ~4 km structurally above the eastern TSZ. Amphibole in sample RS11-113 yielded a pseudo-plateau age of  $1022.3 \pm 7.6$  Ma with a younger perturbation at  $1012.3 \pm 8.0$  Ma (Fig. 12E). Its biotite spectrum defines a plateau at  $930.4 \pm 7.0$  Ma (Fig. 12E). Sample RS11-105 yielded a biotite cooling age of  $905.8 \pm 6.8$  Ma (Fig. 12F).

## 7.3. Interpretation of $^{40}\text{Ar}$ - $^{39}\text{Ar}$ ages

As discussed,  $^{40}\text{Ar}$ - $^{39}\text{Ar}$  ages provide timing constraints on cooling of the area through the closure temperature of amphibole (550-600 °C) and biotite (450 °C). The youngest amphibole ages ( $998.6 \pm 7.4$  Ma and  $1010.0 \pm 7.4$  Ma) were obtained from the interior of the Mékinac-Taureau domain, whereas the oldest ( $\sim 1031.6 \pm 7.6$  Ma) was from the amphibolite located within the eastern TSZ. A sample from the Shawinigan domain yielded an intermediate age of  $1022.3 \pm 7.6$  Ma. Unsurprisingly, all amphibole ages are younger than ~1060 Ma, the age of shearing along the eastern TSZ when rocks were at ~700 °C (see section 6).

An interesting younging trend is identified from the eastern TSZ towards the interior of the

Mékinac-Taureau domain. Amphibole sample RS11-113 located 1 km above the eastern TSZ does not fit in this trend, but the perturbation of its spectrum limits the confidence we have on this date and the interpretations we can make from this sample. Corrigan (1995) explained a similar younging trend from the Tawachiche shear zone towards the Mékinac-Taureau domain by the progressive cooling of the footwall downwards from the detachment surface (e.g. England and Jackson 1987; Hodges et al., 1993; Ruppel et al., 1988). In this study, we have shown the importance of the eastern TSZ for the exhumation of the Mékinac-Taureau domain and consequently propose that cooling may have propagated from this shear zone towards the interior of the Mékinac-Taureau domain, as suggested by the younging trend of amphibole cooling ages in that direction.

Biotite cooling ages vary from ~905 to ~970 Ma and do not show a pattern that is similar to amphibole cooling ages. For samples containing both amphibole and biotite, the time gap between cooling through the  $T_c$  of amphibole and the  $T_c$  of biotite varies from 40 to 90 m.y. This correspond to a cooling rate of 1.36 to 3.10 °C/m.y. for the interval ~1020-920 Ma, assuming closure temperatures of ~575°C and 450 °C for amphibole and biotite, respectively. This is comparable to the cooling rate of 1.1 to 2.5 °C/m.y. calculated by Corrigan (1995) for the interval 1040-990 Ma.

## 8. Discussion

### 8.1. Metamorphic history and timing constraints

This study reveals the presence of the eastern TSZ, a major normal-sense shear zone that separates two domains of contrasting metamorphic history. We conducted conventional thermobarometry on granulites of the Mauricie area because of the evidence for limited to absent effects of retrograde reactions following complete re-equilibration, highlighted by the flat zoning profiles in all garnet grains of this study (Fig. 6). Inasmuch as complete chemical homogenization of garnet requires several tens of m.y. at high temperature (see Caddick et al., 2010), and because it is difficult to ascertain that the calculated P-T conditions truly represent the highest P-T conditions attained by the rocks, results presented herein likely represent metamorphic conditions that prevailed during homogenization and are thus considered minimum estimates of the peak P-T conditions. Our results, summarized in Fig. 13, indicate that rocks in the interior of the Mékinac-Taureau domain located 5.5 km below the eastern TSZ record metamorphic peak conditions of ~1075 MPa and ~825 °C. In the amphibolite sample RS11-082B, collected within the eastern TSZ, P-T values calculated with minerals

interpreted as relict of the former peak assemblage yielded values similar to those calculated in the interior of the domain, whereas P-T values calculated with retrograde minerals interpreted as syn-kinematic with normal shearing yielded P-T values similar to those registered in metapelite from the external zone of the Mékinac-Taureau domain (800 to 650 MPa and 775 to 675 °C). In contrast, metapelite from the Shawinigan domain records P-T conditions varying from 850 to 625 MPa and from 775 to 700 °C. Although evidence for higher metamorphic conditions are lacking, it is impossible to rule out the possibility that these P-T conditions reflects homogenization during retrograde metamorphism from peak conditions similar to that recorded in the Mekinac-Taureau domain. Nevertheless, it is noteworthy that these P-T values are similar to those from the retrogressed metapelite and amphibolite samples of the Mékinac-Taureau domain.

An important finding of this study is the demonstration that the TSZ on the eastern flank of the Mekinac-Taureau domain is a normal shear zone. Its presence is revealed by an increase in qualitative strain, marked by a much better developed stretching lineation and by numerous shear-sense indicators. Timing constraint on the normal-sense shearing along the eastern TSZ is provided by the emplacement of the syn-kinematic pegmatite, RS11-098, that yielded a  $^{207}\text{Pb}/^{206}\text{Pb}$  age of  $1064 \pm 15$  Ma, and for which the temperature of crystallization of zircon ( $\sim 700$  °C  $\pm$  30°C) is consistent with the temperature recorded for retrograde conditions during shearing by the amphibolite RS11-082B ( $720 \pm 60$ °C). Although this age overlaps within errors with that of pegmatite sample RS12-040 from within the Mékinac-Taureau domain, which yielded a  $^{207}\text{Pb}/^{206}\text{Pb}$  age of  $1082 \pm 20$  Ma, the absolute ages of the two pegmatite samples and the difference between them are consistent with previously published ages for the area. Indeed, the minimum age of  $\sim 1082$  Ma for thrust-related deformation and accompanying metamorphism indicated by pegmatite sample RS12-040 is consistent with an age of  $1087 \pm 2$  Ma for a syn-kinematic leucosome from the Shawinigan domain (Corrigan and van Breemen, 1997), whereas the  $\sim 1064$  Ma age for pegmatite sample RS11-098 is consistent with the  $1065 \pm 1$  Ma age for a pegmatite emplaced during normal shearing along the Tawachiche shear zone, located  $\sim 10$  km east of the study area (Fig. 14A; Corrigan and van Breemen, 1997). Although quantitative assessment of the amount of vertical displacement along the eastern TSZ remains impossible with available data, a minimum estimate is provided by the 340 MPa difference in paleopressures (converted to depth by assuming a lithostatic gradient of 30 MPa/km (Winter, 2001)) between peak and retrograde pressure conditions calculated for the amphibolite sample RS11-082B. Consequently, a minimum of  $\sim 11$  km of exhumation occurred during



normal shearing along the eastern TSZ for which the best timing estimate is provided by the ~1064 Ma age of pegmatite RS11-098.

Finally,  $^{40}\text{Ar}/^{39}\text{Ar}$  data on amphibole and biotite provided time constraints on the cooling of the area. Based on amphibole and biotite  $^{40}\text{Ar}/^{39}\text{Ar}$  ages, respectively, the Mauricie area cooled below 550-600 °C at ~1030-1000 Ma and below 450 °C at ~970-900 Ma. Amphibole cooling ages define a younging trend from the eastern TSZ towards the interior of the Mékinac-Taureau domain (Fig. 13).

## 8.2. Mode of exhumation

Exhumation of mid-crustal rocks in the hinterland of orogens can occur in several different tectonic contexts, notably: (1) an orogenic wedge controlled by the critical taper theory, (2) diapirism (e.g. Calvert et al., 1999; Gervais et al., 2004; Teyssier and Whitney, 2002), (3) syn-convergent channel flow (e.g. Beaumont et al., 2001, 2006, Godin et al., 2006) or (4) post-convergent orogenic collapse and metamorphic core complex (MCC) development (e.g. Brun et al., 1994; Rey et al., 2009; Tirel, 2004; Tirel et al., 2004, 2006, 2008). Here, we compare the tectono-metamorphic characteristics of the Mauricie area with distinguishing features expected from these various exhumation modes.

The regional deformation pattern in the Mauricie area is characterized by a dome-shaped foliation pattern parallel to the lithotectonic boundaries and dipping away from the interior of the Mékinac-Taureau domain (Fig. 2). This regional foliation is considered as the result of thrust-related deformation prior to ~1082 Ma in the Mékinac-Taureau domain (this study) and the Shawinigan domain (Corrigan and van Breemen, 1997), although doming of this foliation might be related to the exhumation process. According to Corrigan and van Breemen (1997), thrust faults were located at structural levels above the present exposure of the units. Regional deformation is associated with high-grade metamorphism and partial melting in both domains, migmatites being particularly extensive in the upper structural levels of the Mékinac-Taureau domain. Strain increases in the vicinity of lithotectonic boundaries, i.e. the eastern Taureau and the Tawachiche shear zones. As argued above, the eastern TSZ played a significant role in the exhumation of the Mékinac-Taureau domain at ~1064 Ma. However, the Tawachiche shear zone must also be considered when assessing the exhumation history of the Mauricie area. Corrigan and van Breemen (1997) dated syn- and late-extension pegmatites, constraining NNE-directed extension along the Tawachiche shear zone, between  $1065 \pm 1$  and  $1036 +4/-2$  Ma. Combined with data from our study, this suggests that ESE-directed extension along the eastern TSZ has been

coeval, within uncertainty, with NNE-directed extension along the Tawachiche shear zone. The average directions of tectonic transport on both shear zones are almost at right angle from each other (Fig. 14A). Predominance of normal-sense structures, lack of steep flattening structures and reverse-sense shear zones in the area (e.g. Gervais and Brown, 2011 and references therein), and extensive partial melting of the rock units, limiting the maintenance of a wedge geometry, are all against the orogenic wedge model (Vanderhaeghe et al., 2003). On the other hand, regional foliation conformable to discontinuities and an increase in finite strain towards normal-sense shear zones are structural characteristics common to diapirism, channel flow and MCC formation.

Diapirs are characterized by a radial distribution of stretching lineations, vertical flow in their trunk and horizontal flattening at their apex (e.g. Dixon, 1975). As shown in Fig. 14A, stretching lineations within the TSZ and Tawachiche shear zones flanking the SE and E flanks of the Mékinac-Taureau and Shawinigan domains, respectively, are orthogonal to each other. However, the distribution of these lineations do not correspond to a radial pattern around an hypothetical diapir, but are rather associated with two distinct shear zones located at different structural levels. The interior of the Mékinac-Taureau domain presents a strong foliation dipping away from its core, a feature common to the apex of diapirs. However, relict vertical fabric attesting for vertical flow during diapiric ascent, commonly observed despite the horizontal fabric overprinting (e.g. Gervais et al., 2004), are lacking in the interior of the Mékinac-Taureau domain, despite the ~12 km of vertical section exposed along the tilted transect of the study area. Furthermore, data suggesting an older deformation in the interior of the domain than along the bounding normal-sense shear zones would not be compatible with diapirism. Finally, a buoyancy contrast is required to initiate and maintain diapirism (Teyssier and Whitney, 2002). In the Mauricie area, it is not clear whether the relatively small area of garnet-rich metapelite in the St-Boniface paragneiss and of mafic volcanic rocks in the Portneuf-Mauricie domain constituted a sufficient volume of dense rocks to initiate diapirism. Due to poor compatible structural evidence, apparently incompatible timing of deformation and lack of an obvious efficient driving mechanism, diapirism is not proposed as the exhumation process for the Mauricie area.

Extrusion of mid-crustal material by channel flow involves a melt-weakened ductile layer bounded by a thrust shear zone below and a normal shear zone above (Godin et al., 2006). Key characteristics of such model that are testable in the study area include: 1) high shear strain commonly distributed

through the channel; 2) coeval reverse- and normal-sense shearing at the base and top of the channel, respectively; 3) uniform cooling ages at any transverse sections of the channel and progressively older cooling ages from the front towards the rear of the channel (Gervais and Brown, 2011; Godin et al., 2006). If such a mechanism occurred in the Mauricie area, the eastern TSZ would be the upper normal-sense shear zone and the underlying Mekinac-Taureau domain would be the upper portion of the channel. Although deformation within the latter is interpreted as resulting from NW thrusting, the variable and poorly developed lineation (Fig. 2) does not suggest high shear strain. Furthermore, although more robust geochronological data would be desirable, available data suggest that penetrative deformation within the putative channel occurred prior to ~1082 Ma, whereas normal shearing along its upper shear zones, the eastern TSZ and the Tawachiche shear zone, was occurring at ~1064 Ma and probably continued until 1036 Ma, the age of a “late-extensional” pegmatite emplaced within the Tawachiche shear zone (Corrigan and van Breemen, 1997). Evidence for synchronicity of reverse- and normal-sense shearing, characteristic 2 above, is therefore lacking. Finally, as a channel flows towards the surface, its frontal part should cool before its rear. The trend of hornblende argon cooling age decreasing towards the core of the Mekinac-Taureau domain could be compatible with this characteristic, although it could also reflect a trend towards deeper structural levels. Consequently, although more data are needed, especially at the northern end of the Mekinac-Taureau domain, available data from the Mauricie area do not seem to support the channel flow hypothesis as a single exhumation mechanism. The possibility of an earlier phase of mid-crustal flow overprinted by another mechanism cannot however be entirely excluded.

Metamorphic core complexes are characterized by a dome of high-grade metamorphic rocks in the footwall, covered by non-metamorphic upper crustal units (or units that have experienced an earlier metamorphic event) in the hanging wall of a normal-sense shear zone, which is generally planar or slightly convex upward at the apex of the dome and dips away from that dome on its flanks (e.g. Lister and Davis, 1989; Tírel 2006; Wernicke, 1985). In the Mauricie area, the Mékinac-Taureau domain underwent high-grade metamorphism before 1082 Ma (1075 MPa and ~825 °C; this study) and the Shawinigan domain underwent coeval and slightly lower-grade metamorphism (625-850 MPa and 700-775 °C, this study; Corrigan and van Breemen, 1997). In contrast, peak metamorphic conditions in the overlying Portneuf-Mauricie domain was significantly lower (300-600 MPa and 550-700 °C; Corrigan, 1995; Lévesque, 1995) and most likely much older (estimated at ~1400 Ma by Corrigan and van

973 Breemen, 1997). This geometry of domains of contrasted metamorphic grades separated by gently  
974 dipping ( $\sim 20\text{--}30^\circ$ ) normal-sense shear zones that were active after the main episode of deformation and  
975 metamorphism in the dome core are compatible to that expected on the flank of a MCC, although two  
976 major normal shear zones are present, instead of a single decollement horizon (Fig. 14C). Furthermore,  
977 the late, brittle-ductile normal faults observed in the Shawinigan domain, south of the TSZ (i.e.  
978 structurally above the shear zone; Fig. 4B) could be compatible with the synthetic structures related to  
979 the main detachment commonly observed in the hanging walls of MCCs (e.g. Wernicke, 1985). The top  
980 bounding shear zone of MCCs is commonly retrograde when compared with the metamorphic grade of  
981 the footwall (Dallmeyer et al. 1986; Gibson et al. 1988; Lister and Davis, 1989). This is the case for the  
982 eastern TSZ, where retrograde metamorphic textures and retrograde P-T conditions were observed in an  
983 amphibolite sampled within the shear zone. Corrigan (1995) and Corrigan and van Breeman (1997) also  
984 suggested that the Tawachiche shear zone was retrograde as compared to peak metamorphism in the  
985 underlying Shawinigan domain. The trend of cooling ages younging towards the core of the dome is a  
986 feature uncommon to classic metamorphic core complexes (e.g. Sullivan and Snooke, 2007), but similar  
987 cooling trends are nevertheless reported in the literature (e.g. Brun and Sokoutis, 2007) and can be  
988 inferred from results of numerical modeling (Tirel et al. 2008). MCC development is commonly  
989 associated with unidirectional direction of extension (e.g. Doughty et al., 2007; Lana et al., 2010; Lister  
990 and Davis, 1989), as opposed to the orthogonal trends of stretching lineation associated with the  
991 Tawachiche and eastern TSZ (Fig. 14A). Although uncommon, examples of core complexes with  $>1$   
992 directions of extension however exist in nature. Hill et al., (1992) and Hill (1994), for instance, described  
993 the d'Entrecasteaux Island MCC and argued for the existence of bounding shear zones with directions of  
994 shearing at  $90^\circ$  from one another. Although present data suggest that the eastern Taureau and  
995 Tawachiche shear zones are coeval within uncertainty, the possibility of temporally discrete phases with  
996 orthogonal direction of extension cannot be firmly ruled out. Whether both shear zones were coeval or  
997 not, this pattern is best explained if orogenic collapse was of the gravity-driven fixed-boundary mode (as  
998 in the terminology of Rey et al., 2001) in contrast to the free-boundary mode of most cordilleran MCC  
999 that formed in a regional tensional stress regime. The fixed mode is driven by vertical  $\sigma_1$  due to  
1000 gravitational forces rather than by horizontal, orogen-perpendicular tension along  $\sigma_3$ . In 3D, the fixed  
1001 mode should result in  $\sigma_2 \approx \sigma_3$  and, in turn, could explain the pattern of orthogonal lineations observed  
1002 in the normal-sense shear zones bounding the complex. A quasi radial pattern of extension is also  
1003 observed at the scale of the Grenville Province (Rivers; 2012). Furthermore, a MCC not developing by a

rolling-hinge mechanism (Axen and Bartley, 1997) could potentially explain the difference in trends of cooling ages as well. Even if some characteristics of the Mauricie area do not correspond to that of a typical cordilleran MCC, we consider that gravitational collapse is the most likely mechanism of exhumation of the Mékinac-Taureau domain. The possibility of an earlier phase of mid-crustal flow preceding the gravitational collapse cannot be confidently ruled out, but data suggest that channel flow alone cannot explain the geological architecture observed in the Mauricie area. Results of this study, therefore, support the conceptual model of gravitational collapse presented by Rivers (2008, 2012).

## 9. Conclusions

Structural analysis, thermobarometry, U-Pb and  $^{40}\text{Ar}/^{39}\text{Ar}$  geochronology on selected samples of the Mauricie area provided data essential to the reconstruction of the tectono-metamorphic history of the area:

- 1) Peak metamorphism in the Mékinac-Taureau domain reached P-T conditions of 1000-1100 MPa and 820-880 °C prior to  $1082 \pm 20$  Ma. This metamorphic event is considered as the result of northwestward thrusting and regional-scale crustal thickening.
- 2) Retrograde conditions varying from 800 to 650 MPa and from 775 to 675 °C were recorded in the upper structural levels of the Mékinac-Taureau domain.
- 3) The Shawinigan domain records P-T conditions varying from 850 to 625 MPa and from 775 to 700 °C, values that are equivalent or of a slightly lower metamorphic grade as compared with retrogressed samples from the margin of the Mékinac-Taureau domain.
- 4) The contact between the Mékinac-Taureau and the Shawinigan domains is marked by a normal-sense shear zone with a top-down-to-the-ESE sense of shear, the eastern TSZ, that was active at  $\sim 1064 \pm 15$  Ma, during and/or after retrograde metamorphism documented in the Mékinac-Taureau domain.
- 5) Normal-sense shearing along the eastern TSZ is coeval, within uncertainty, with NNE-directed normal-sense shearing along the Tawachiche shear zone (Corrigan, 1995; Corrigan and van Breemen, 1997).
- 6) The area cooled below 550-600 °C at  $\sim 1000$ -1030 Ma and below 450 °C at  $\sim 900$ -970 Ma.
- 7) Structural and metamorphic characteristics of the Mauricie area are similar to those expected from a metamorphic core complex formed during post-convergent orogenic collapse in a gravity-driven fixed-boundary mode. The Mékinac-Taureau and Shawinigan domains were thus probably exhumed by a similar process. Our study thus supports the orogenic collapse

1035 model of Rivers (2008, 2012) for the exhumation of mid-crustal metamorphic core complexes  
1036 in the Grenville Province.

## 1037 **Acknowledgments**

1038 This work is part of a M.Sc. thesis undertaken by Renaud Soucy La Roche at Université du Québec  
1039 à Montréal (UQÀM). Renaud Soucy La Roche received graduate scholarships from the Natural Sciences  
1040 and Engineering Research Council of Canada (NSERC) and the Fonds de recherche du Québec – Nature  
1041 et Technologies (FRQNT). The project was financed by a NSERC research grant held by Alain Tremblay  
1042 (PG 105669) and by internal funding provided to Félix Gervais by École Polytechnique de Montréal.  
1043 Morgann Perrot and Xavier Vasseaud are thanked for field assistance. Lang Shi from the Electron  
1044 Microprobe Laboratory of the McGill University is thanked for his assistance during the acquisition of  
1045 mineral chemical compositions for thermobarometry. Michelle Laithier is also thanked for her useful  
1046 advices on figures conception. A previous version of this manuscript benefited from comments by  
1047 Alexandre Zagorevski and Léopold Nadeau. We also thank Toby Rivers and Aphrodite Indares for  
1048 critical, but constructive, reviews of the manuscript and Randall Parrish for editorial handling.

## 1049 **References**

- 1050 Allaz, J., 2008. *Metamorphic evolution in the northern Central Alps: linking  $^{39}\text{Ar}$ - $^{40}\text{Ar}$  dating with*  
1051 *thermobarometry* (Ph.D. thesis). Universität Bern, Bern, Switzerland, 224 pp.
- 1052 Allaz, J., Engi, M., Berger, A., Villa, I.M., 2011. The Effects of Retrograde Reactions and of Diffusion on  
1053  $^{40}\text{Ar}$ - $^{39}\text{Ar}$  Ages of Micas. *Journal of Petrology*, 52(4), 691-716.
- 1054 Axen, G.J., Bartley, J.M. 1997. Field tests of rolling hinges: Existence, mechanical types, and implications  
1055 for extensional tectonics. *Journal of Geophysical Research: Solid Earth*, 102(B9), 20515-20537.
- 1056 Barton, J.M.Jr., Doig, R., 1972. Rb-Sr Isotopic studies of the Lac Croche Complex, Grenville Province,  
1057 Quebec. *Canadian Journal of Earth Sciences*, 9(9), 1180-1186.
- 1058 Beaumont, C.J., Jamieson, R.A., Nguyen, M.H., Lee, B., 2001. Himalayan tectonics explained by extrusion  
1059 of a low-viscosity crustal channel coupled to focused surface denudation. *Nature*, 414(6865), 738-  
1060 742.
- 1061 Beaumont, C.J., Nguyen, M. H., Jamieson, R. A., Ellis, S., 2006. Crustal flow modes in large hot orogens.  
1062 *Geological Society, London, Special Publications*, 268(1), 91-145.
- 1063 Berman, R.G., 1988. Internally-consistent thermodynamic data for stoichiometric minerals in the system  
1064  $\text{K}_2\text{O}-\text{Na}_2\text{O}-\text{CaO}-\text{MgO}-\text{FeO}-\text{Fe}_2\text{O}_3-\text{Al}_2\text{O}_3-\text{SiO}_2-\text{TiO}_2-\text{H}_2\text{O}-\text{CO}_2-\text{O}$ . *Journal of Petrology*, 29(2), 445-522.
- 1065 Berman, R.G., 1991. Thermobarometry using multi-equilibrium calculations: a new technique, with  
1066 petrological applications. *Canadian Mineralogist*, 29(4), 833-855.
- 1067 Berman, R.G., 2007. winTWQ (version 2.3): A software package for performing internally-consistent

- thermobarometric calculations. *Geological Survey of Canada, Open File*, 5462 (revised).
- Berman, R.G., Aranovich, L.Y., Rancourt, D.G., Mercier, P.H.J., 2007. Reversed phase equilibrium constraints on the stability of Mg-Fe-Al biotite. *American Mineralogist*, 92, 139-150.
- Brun, J. P., Sokoutis, D., 2007. Kinematics of the southern Rhodope core complex (North Greece). *International Journal of Earth Sciences*, 96(6), 1079-1099.
- Brun, J.P., Sokoutis, D., van den Driessche, J., 1994. Analogue modeling of detachment fault systems and core complexes. *Geology*, 22(4), 319-322.
- Caddick, M.J., Konopasek, J., Thompson, A.B., 2010. Preservation of garnet growth zoning and the duration of prograde metamorphism. *Journal of petrology*, 51(11), 2327-2347.
- Calvert, A.T., Gans, P.B., Amato, J.M., 1999. Diapiric ascent and cooling of a sillimanite gneiss dome revealed by  $^{40}\text{Ar}/^{39}\text{Ar}$  thermochronology: the Kigluaik Mountains, Seward Peninsula, Alaska. *Geological Society, London, Special Publications*, 154(1), 205-232.
- Carmichael, D.M. 1978. Metamorphic bathozones and bathograds; a measure of the depth of post-metamorphic uplift and erosion on the regional scale. *American Journal of Science*, 278(6), 769-797.
- Cathelineau M., Boiron M.C., Fourcade S., Ruffet G., Clauer N., Belcourt O., Coulibaly Y., Banks D.A., Guillocheau F., 2012. A major Late Jurassic fluid event at the basin/basement unconformity in western France:  $^{40}\text{Ar}/^{39}\text{Ar}$  and K-Ar dating, fluid chemistry, and related geodynamic context. *Chemical Geology*, 322-323, 99-120.
- Corfu F., Hanchar, J.M., Hoskin, P.W.O., Kinny, P., 2003. Atlas of zircon textures. *Reviews in Mineralogy and Geochemistry*, 53(1), 469-500.
- Corrigan, D. 1995. *Mesoproterozoic evolution of the south-central Grenville orogen: structural, metamorphic, and geochronologic constraints from the Mauricie transect* (Ph.D. thesis). Carleton University, Ottawa, Canada, 308 pp.
- Corrigan, D., van Breemen, O., 1997. U-Pb age constraints for the lithotectonic evolution of the Grenville Province along the Mauricie transect, Québec. *Canadian Journal of Earth Sciences*, 34(3), 299-316.
- Dahl, P.S., 1996. The effects of composition on retentivity of argon and oxygen in hornblende and related amphiboles: a field-tested empirical model. *Geochimica et Cosmochimica Acta*, 60(19), 3687-3700.
- Dahlen, F.A., 1990. Critical taper model of fold-and-thrust belts and accretionary wedges. *Annual Review of Earth and Planetary Sciences*, 18, 55-99.
- Dale, J., Powell, R., White, R.W., Elmer, F.L., Holland, T.J.B., 2005. A thermodynamic model for Ca-Na clinoamphiboles in Na<sub>2</sub>O-CaO-FeO-MgO-Al<sub>2</sub>O<sub>3</sub>-SiO<sub>2</sub>-H<sub>2</sub>O-O for petrological calculations. *Journal of Metamorphic Geology*, 23(8), 771-791.
- Dallmeyer, R.D., Snoke, A.W., McKee, E.H., 1986. The Mesozoic-Cenozoic tectonothermal evolution of the Ruby Mountains, East Humboldt Range, Nevada: A Cordilleran Metamorphic Core Complex. *Tectonics*, 5(6), 931-954.
- Davidson, C., Schmid, S.M., Hollister, L.S., 1994. Role of melt during deformation in the deep crust. *Terra Nova*, 6(2), 133-142.
- Dewey, J.F., 1988. Extensional collapse of orogens. *Tectonics*, 7(6), 1123-1139.
- Dewey, J.F., Burke, K.C., 1973. Tibetan, Variscan, and Precambrian basement reactivation: products of continental collision. *The Journal of Geology* 81(6), 683-692.
- Dixon, J. M., 1975. Finite strain and progressive deformation in models of diapiric structures.

- 1110 *Tectonophysics*, 28(1), 89-124.
- 1111 Dodson, M.H., 1973. Closure temperature in cooling geochronological and petrological systems.
- 1112 *Contributions to Mineralogy and Petrology*, 40(3), 259-274.
- 1113 Doig, R., 1991. U-Pb zircon dates of Morin Anorthosite suite rocks, Grenville Province, Quebec. *Journal*
- 1114 *of Geology*, 99(5), 729-738.
- 1115 Doughty, P.T., Chamberlain, K.R., Foster, D.A., Grant, S.S., 2007. Structural, metamorphic, and
- 1116 geochronologic constraints on the origin of the Clearwater core complex, northern Idaho. *Geological*
- 1117 *Society of America Special Papers*, 433, 211-241.
- 1118 England, P., Jackson, J., 1987. Migration of the seismic-aseismic transition during uniform and
- 1119 nonuniform extension of the continental lithosphere. *Geology*, 15(4), 291-294.
- 1120 England, P., Molnar, P., 1990. Surface uplift, uplift of rocks, and exhumation of rocks. *Geology*, 18(12),
- 1121 1173-1177.
- 1122 Essene, J.E., 1989. The current status of thermobarometry in metamorphic rocks. *Geological Society,*
- 1123 *London, Special Publication*, 43(1), 1-44.
- 1124 Ferriss, E.D.A., Essene, E.J., Becker, U., 2008. Computational study of the effect of pressure on the Ti-in-
- 1125 zircon geothermometer. *European Journal of Mineralogy*, 20(5), 745-755.
- 1126 Ferry, J.M., Watson, E.B., 2007. New thermodynamic models and revised calibrations for the Ti-in-zircon
- 1127 and Zr-in-rutile thermometers. *Contributions to Mineralogy and Petrology*, 154(4), 429-437.
- 1128 Fortier, S.M., Giletti, B.J., 1989. An empirical model for predicting diffusion coefficients in silicate
- 1129 minerals. *Science*, 245(4925), 1481-1484.
- 1130 Friedman, R.M., Martignole, J., 1995. Mesoproterozoic sedimentation, magmatism, and metamorphism
- 1131 in the southern part of the Grenville Province (western Quebec): U-Pb geochronological constraints.
- 1132 *Canadian Journal of Earth Sciences*, 32(12), 2103-2114.
- 1133 Fuhrman, M.L., Lindsley, D.H., 1988. Ternary-feldspar modeling and thermometry. *The American*
- 1134 *Mineralogist*, 73(3-4), 201-216.
- 1135 Gapais, D., Cagnard, F., Gueydan, F., Barbey P., Ballèvre M., 2009. Mountain building and exhumation
- 1136 processes through time: inferences from nature and models. *Terra Nova*, 21(3), 188-194.
- 1137 Gervais, F., Brown, R.L., 2011. Testing modes of exhumation in collisional orogens: Synconvergent
- 1138 channel flow in the southeastern Canadian Cordillera. *Lithosphere*, 3(1), 55-75.
- 1139 Gervais, F., Nadeau, L., Malo, M., 2004. Migmatitic structures and solid-state diapirism in orthogneiss
- 1140 domes, eastern Grenville Province, Canada. *Geological Society of America Special Papers*, 380, 359-
- 1141 378.
- 1142 Gerya, T.V., Perchuk, L.L., Maresch, W.V., Willner, A.P., 2004. Inherent gravitational instability of hot
- 1143 continental crust: Implications for doming and diapirism in granulite facies terrains. *Geological*
- 1144 *Society of America Special Papers*, 380, 97-115.
- 1145 Gibson, G.M., McDougall, I., Ireland, T.R., 1988. Age constraints on metamorphism and the development
- 1146 of a metamorphic core complex in Fiordland, southern New Zealand. *Geology*, 16(5), 405-408.
- 1147 Godin, L., Grujic, D., Law, R.D., Searle, M.P., 2006. Channel flow, ductile extrusion and exhumation in
- 1148 continental collision zones: an introduction. *Geological Society, London, Special Publications*, 268(1),
- 1149 1-23.
- 1150 Goodspeed, G. E., 1940. Dilation and replacement dikes. *The Journal of Geology*, 175-195.



- 1151 Grove, T.L., Baker, M.B., Kinzler, R.J., 1984. Coupled CaAl-NaSi diffusion in plagioclase feldspar:  
1152 Experiments and applications to cooling rate speedometry. *Geochimica et Cosmochimica Acta*,  
1153 48(10), 2112-2121.
- 1154 Hanmer, S., 1988. Ductile thrusting at mid-crustal level, southwestern Grenville Province, *Canadian*  
1155 *Journal of Earth Sciences*, 25(5), 1049- 1059.
- 1156 Hanmer, S., Passchier, C., 1991. *Shear-sense indicators: A review*. Ottawa: Geological Survey of Canada,  
1157 72 pp.
- 1158 Harrison, T.M., 1981. Diffusion of  $^{40}\text{Ar}$  in hornblende. *Contribution to Mineralogy and Petrology*, 78(3),  
1159 324-331.
- 1160 Harrison, T.M., Duncan, I., McDougall, I., 1985. Diffusion of  $^{40}\text{Ar}$  in biotite: temperature, pressure and  
1161 compositional effects. *Geochimica et Cosmochimica Acta*, 49(11), 2461-2468.
- 1162 Hauzenberger, C.A., Robl, J., Stüwe, K., 2005. Garnet zoning in high pressure granulite-facies  
1163 metapelites, Mozambique belt, SE-Kenya constraints on the cooling history. *European journal of*  
1164 *mineralogy*, 17(1), 43-55.
- 1165 Hayden L.A., Watson E.B., 2007. Rutile saturation in hydrous siliceous melts and its bearing on Ti  
1166 thermometry of quartz and zircon. *Earth and Planetary Sciences Letters*, 258(3), 561-568
- 1167 Henry, D.J., Guidotti, C.V., Thomson, J.A., 2005. The Ti-saturation surface for low-to-medium pressure  
1168 metapelitic biotites: Implications for geothermometry and Ti-substitution mechanisms. *American*  
1169 *Mineralogist*, 90(2-3), 316-328.
- 1170 Herd, K., Ackerman, D., Windley, B.F., Rondot, J., 1986. Sapphirine-garnet rocks, St. Maurice area,  
1171 Québec: petrology and implications for tectonics and metamorphism. *Geological Association of*  
1172 *Canada, Special Paper*, 31, 241-253.
- 1173 Hill, E.J., 1994. Geometry and kinematics of shear zones formed during continental extension in eastern  
1174 Papua New Guinea. *Journal of Structural Geology*, 16(8), 1093-1105.
- 1175 Hill, E.J., Baldwin, S.L., Lister, G.S., 1992. Unroofing of active metamorphic core complexes in the  
1176 D'Entrecasteaux Islands, Papua New Guinea. *Geology*, 20(10), 907-910.
- 1177 Hocq, M., Dufour S., 2002. Compilation Géologique – *Réservoir Taureau*. Québec: Ministère des  
1178 Ressources Naturelles et de la Faune.
- 1179 Hocq, M., Dufour S., 1999. Compilation Géologique – *Lac Éveline*. Québec: Ministère des Ressources  
1180 Naturelles et de la Faune.
- 1181 Hodges, K.V., Burchfiel, B.C., Royden, L.H., Chen, Z., Liu, Y., 1993. The metamorphic signature of  
1182 contemporaneous extension and shortening in the central Himalayan orogen: data from the Nyalam  
1183 transect, southern Tibet. *Journal of Metamorphic Geology*, 11(5), 721-737.
- 1184 Holdaway, M.J., 2001. Recalibration of the GASP geobarometer in light of recent garnet and plagioclase  
1185 activity models and versions of the garnet-biotite geothermometer. *American Mineralogist*, 86(10),  
1186 1117-1129.
- 1187 Holland, T.J.B., Powell, R., 1998. An internally consistent thermodynamic data set for phases of  
1188 petrological interest. *Journal of metamorphic Geology*, 16(3), 309-343.
- 1189 Hoskin, P.W.O., Black, L.P., 2000. Metamorphic zircon formation by solid-state recrystallization of  
1190 protolith igneous zircon. *Journal of Metamorphic Geology*, 18(4), 423-439.
- 1191 Hoskin, P.W.O., Shaltegger, U., 2003. The composition of zircon and igneous and metamorphic  
1192 petrogenesis. *Reviews in Mineralogy and Geochemistry*, 53(1), 27-62.

- 1193 Hynes, A., Rivers, T., 2010. Protracted continental collision evidence from the Grenville Orogen.  
1194 *Canadian Journal of Earth Sciences*, 47(5), 591-620.
- 1195 Jamieson, R.A., Beaumont, C., Nguyen, M.H., Culshaw, N.G., 2007. Synconvergent ductile flow in  
1196 variable-strength continental crust: numerical models with application to the western Grenville  
1197 orogen. *Tectonics*, 26(5), TC5005.
- 1198 Jamieson, R.A., Beaumont, C., Warren, C.J., Nguyen, M.H., 2010. The Grenville Orogen explained?  
1199 Applications and limitations of integrating numerical models with geological and geophysical data.  
1200 *Canadian Journal of Earth Sciences*, 47(4), 517-539.
- 1201 Jourdan, F., Renne, P.R., 2007. Age calibration of the Fish Canyon sanidine  $^{40}\text{Ar}/^{39}\text{Ar}$  dating standard  
1202 using primary K-Ar standards. *Geochimica Cosmochimica Acta*, 71(2), 387-402.
- 1203 Jourdan, F., Verati, C., Féraud, G., 2006. Intercalibration of the Hb3gr  $^{40}\text{Ar}/^{39}\text{Ar}$  dating standard. *Chemical*  
1204 *Geology*, 231(3), 77-189.
- 1205 Kohn, M.J., Spear, F., 2000. Retrograde net transfer reaction insurance for pressure-temperature  
1206 estimates. *Geology*, 28(12), 1127-1130.
- 1207 Kretz, R., 1983. Symbols for rock-forming minerals. *American Mineralogist*, 68, 277-279.
- 1208 Lana, C., Kisters, A., Stevens, G., 2010. Exhumation of Mesoarchean TTG gneisses from the middle crust:  
1209 Insights from the Steynsdorp core complex, Barberton granitoid-greenstone terrain, South Africa.  
1210 *Geological Society of America Bulletin*, 122(1-2), 183-197.
- 1211 Leake, B.E., 1978. Nomenclature of amphiboles. *Canadian Mineralogist*, 14(4), 501-520.
- 1212 Lee, J.Y., Marti, K., Severinghaus, J.P., Kawamura, K., Yoo, H.S., Lee, J.B., Kim, J.S., 2006. A  
1213 redetermination of the isotopic abundances of atmospheric Ar. *Geochimica et Cosmochimica*  
1214 *Acta*, 70(17), 4507-4512.
- 1215 Lemieux, É.B., 1992. *Analyse structurale de la partie nord du groupe de Montauban, province de*  
1216 *Grenville* (M.Sc. thesis). Université Laval, Québec, Canada.
- 1217 Lévesque, S., 1995. *Zonation métamorphique et évolution thermique de la région Portneuf-Mauricie,*  
1218 *orogène de Grenville* (M.Sc. thesis). Université Laval, Québec, Canada.
- 1219 Lister, G.S., Davis, G.A., 1989. The origin of metamorphic core complexes and detachment faults formed  
1220 during Tertiary continental extension in the northern Colorado River region, USA. *Journal of*  
1221 *Structural Geology*, 11(1), 65-94.
- 1222 Ludwig, K.R., 2003. *User's Manual for Isoplot 3.00*. Berkeley: Geochronology Center.
- 1223 Mäder, U.K., Percival, J.A., Berman, R.G., 1994. Thermobarometry of garnet-clinopyroxene-hornblende  
1224 granulites from the Kapuskasing structural zone, *Canadian Journal of Earth Sciences*, 31(7), 1134-  
1225 1145.
- 1226 Mark, D.F., Stuart, F.M., De Podesta, M., 2011. New high-precision measurements of the isotopic  
1227 composition of atmospheric argon. *Geochimica et Cosmochimica Acta*, 75(23), 7494-7501.
- 1228 Martignole, J., 1975. *Le Précambrien dans le sud de la province tectonique de Grenville (Bouclier*  
1229 *Canadien)* (Doctorat d'état thesis). Université Paul Sabatier, Toulouse, France, 242 pp.
- 1230 Martignole, J., Friedman, R., 1998. Geochronological constraints on the last stages of terrane assembly  
1231 in the central part of the Grenville Province. *Precambrian Research*, 92(2), 145-164.
- 1232 Nadeau, L., Brouillette, P., 1994. Structural map of the La Tuque area (NTS 31P), Grenville Province,  
1233 Quebec. *Geological Survey of Canada, Open File 2938*, échelle 1: 250 000.

- 1234 Nadeau, L., Brouillette, P., 1995. Structural map of the Shawinigan area (NTS 31I), Grenville Province,  
1235 Quebec. *Geological Survey of Canada, Open File 3012*, échelle 1: 250 000.
- 1236 Nadeau, L., Brouillette, P., Hébert, C., 2009. *Geological compilation map of the Portneuf-St.Maurice*  
1237 *region, Grenville Province, Quebec* (GM 63830). Québec: Ministère des Ressources Naturelles et de la  
1238 Faune.
- 1239 Nadeau, L., Corrigan, D., 1991. Preliminary notes of the geology of the St-Maurice tectonic zone,  
1240 Grenville orogen, Quebec. *Geological Survey of Canada, Current research*, E, 245-255.
- 1241 Nadeau, L., Van Breemen, O., 2001. U-Pb Zircon Age and Regional Setting of the Lapeyrère  
1242 Gabbonorite, Portneuf-Mauricie Region, South Central Grenville Province, Quebec. *Geological*  
1243 *Survey of Canada, Current research, part F6*, 1-8.
- 1244 Nadeau, L., van Breemen, O., 1994. *Do the 1.45-1.39 Ga Montauban group and the La Bostonnais*  
1245 *complex constitute a Grenvillian accreted terrane?* Geological Association of Canada – Mineralogical  
1246 Association of Canada annual meeting, Waterloo, abstract volume 19: A81.
- 1247 Passchier, C. W., Trouw, R.A.J., 2005. *Microtectonics* (2<sup>e</sup> éd.). Berlin: Springer, 366 pp.
- 1248 Pattison, D.R.M., 1992. Stability of andalusite and sillimanite and the  $\text{Al}_2\text{SiO}_5$  triple point: constraints  
1249 from the Ballachulish aureole. *The Journal of Geology*, 100(4), 423-446.
- 1250 Pan, Y., 1997. Zircon- and monazite-forming metamorphic reactions at Manitouwadge, Ontario. *The*  
1251 *Canadian Mineralogist*, 35(1), 105-118.
- 1252 Peck, W.H., DeAngelis, M.T., Meredith, M.T., Morin, E., 2005. Polymetamorphism of marbles in the  
1253 Morin terrane, Grenville Province, Quebec. *Canadian Journal of Earth Sciences*, 42(10), 1949-1965.
- 1254 Peck, W.H., 2012. Reconnaissance geochronology and geochemistry of the Mont-Tremblant gneiss of  
1255 the Morin terrane, Grenville Province, Québec. *Geosphere*, 8(6): 1356-1365.
- 1256 Platt, J.P., 1986. Dynamics of orogenic wedges and the uplift of high-pressure metamorphic  
1257 rocks. *Geological Society of America Bulletin*, 97(9), 1037-1053.
- 1258 Powell, R., Holland, T.J.B., 1988. An internally consistent dataset with uncertainties and correlations: 3.  
1259 Applications to geobarometry, worked examples and a computer program. *Journal of Metamorphic*  
1260 *Geology*, 6(2), 173-204.
- 1261 Powell, R., Holland, T.J.B., 1994. Optimal geothermometry and geobarometry. *American Mineralogist*,  
1262 79(1-2), 120-133.
- 1263 Powell, R., Holland, T.J.B., 2008. On thermobarometry. *Journal of Metamorphic Geology*, 26(2), 155-179.
- 1264 Renne, P.R., Balco, G., Ludwig, R.L., Mundil, R., Min. K., 2011. Response to the comment by W.H.  
1265 Schwarz et al., on “Joint determination of  $^{40}\text{K}$  decay constants and  $^{40}\text{Ar}^*/^{40}\text{K}$  for the Fish Canyon  
1266 sanidine standard, and improved accuracy for  $^{40}\text{Ar}/^{39}\text{Ar}$  geochronology” by PR Renne et al. (2010).  
1267 *Geochimica et Cosmochimica Acta*, 75(17), 5097-5100.
- 1268 Renne, P.R., Mundil, R., Balco, G., Min, K., Ludwig R.L., 2010. Joint determination of  $^{40}\text{K}$  decay constants  
1269 and  $^{40}\text{Ar}^*/^{40}\text{K}$  for the Fish Canyon sanidine standard, and improved accuracy for  $^{40}\text{Ar}/^{39}\text{Ar}$   
1270 geochronology. *Geochimica et Cosmochimica Acta* 74(18), 5349-5367.
- 1271 Rey, P.F., Teyssier, C., Whitney, D.L., 2009. Extension rates, crustal melting, and core complex dynamics.  
1272 *Geology*, 37(5), 391-394.
- 1273 Rey, P.F., Vanderhaeghe, O., Teyssier, C., 2001. Gravitational collapse of the continental crust:  
1274 Definition, regimes and modes. *Tectonophysics*, 342(3), 435-449.
- 1275 Ring, U., Brandon, M.T., Lister, G.S., Willet, S.D., 1999. Exhumation Processes. *Geological Society*,

- 1276      *London, Special Publications, 154, 1-27.*
- 1277      Rivers, T., 1997. Lithotectonic elements of the Grenville Province: review and tectonic implications.  
1278      *Precambrian Research, 86(3), 117-154.*
- 1279      Rivers, T., 2008. Assembly and preservation of lower, mid and upper orogenic crust in the Grenville  
1280      Province — Implications for the evolution of large, hot long-duration orogens. *Precambrian Research,*  
1281      *167(3), 237-259.*
- 1282      Rivers, T., 2009. The Grenville Province as a large hot long-duration collisional orogen — insights from  
1283      the spatial and thermal evolution of its orogenic fronts. *Geological Society, London, Special*  
1284      *Publication 327(1), 405-444.*
- 1285      Rivers, T., 2012. Upper-crustal orogenic lid and mid-crustal core complexes: signature of a collapsed  
1286      orogenic plateau in the hinterland of the Grenville Province. *Canadian Journal of Earth Sciences,*  
1287      *49(1), 1-42.*
- 1288      Rivers, T., Martignole, J., Gower, C.F., Davidson, A., 1989. New tectonic divisions of the Grenville  
1289      Province, southeast Canadian shield. *Tectonics, 8(1), 63-84.*
- 1290      Rivers, T., Culshaw, N., Hynes, A., Indares, A., Jamieson, R., & Martignole, J. (2012). The Grenville  
1291      Orogen—A post-Lithoprobe perspective. *Tectonic styles in Canada: The LITHOPROBE perspective. In*  
1292      *tectonic styles in Canada: the Lithoprobe perspective. Edited by JA Percival, FA Cook, and RM Clowes.*  
1293      *Geological Association of Canada Special Paper, 49, 97-238.*
- 1294      Robinson, P., Spear, F.S., Schumacher, J.C., Laird, J., Klein, C., Evans, B.W., Doolan, B.L., 1982. Phase  
1295      relations of metamorphic amphiboles: natural occurrence and theory. *Reviews in Mineralogy and*  
1296      *Geochemistry, 9(1), 1-211.*
- 1297      Roddick, J.C., 1983. High precision intercalibration of  $^{40}\text{Ar}/^{39}\text{Ar}$  standards. *Geochimica et Cosmochimica*  
1298      *Acta, 47(5), 887-898.*
- 1299      Rosenberg, C.L., Handy, M.R., 2005. Experimental deformation of partially melted granite revisited:  
1300      implications for the continental crust. *Journal of Metamorphic Geology, 23(1), 19-28.*
- 1301      Royden, L., 1996. Coupling and decoupling of crust and mantle in convergent orogens: Implications for  
1302      strain partitioning in the crust. *Journal of Geophysical Research: Solid Earth, 101(B8), 17679-17705.*
- 1303      Ruffet, G., Féraud, G., Amouric, M., 1991. Comparison of  $^{40}\text{Ar}/^{39}\text{Ar}$  conventional and laser dating of  
1304      biotites from the North Trégor Batholith. *Geochimica et Cosmochimica Acta, 55(6), 1675-1688.*
- 1305      Ruffet, G., Féraud, G., Ballèvre, M., Kiénaast, J.R., 1995. Plateau ages and excess argon on phengites: a  
1306       $^{40}\text{Ar}/^{39}\text{Ar}$  laser probe study of alpine micas (Sesia zone). *Chemical Geology, 121(11), 327-343.*
- 1307      Ruppel, C., Royden, L., Hodges, K.V., 1988. Thermal modeling of extensional tectonics: application to  
1308      pressure-temperature-time histories of metamorphic rocks. *Tectonics, 7(5), 947-957.*
- 1309      Schaub, P.M., Carr, S.D., Berman, R.G., 2002. Structural and metamorphic constraints on ca. 70Ma  
1310      deformation of the northern Valhalla complex, British Columbia: implications for the tectonic  
1311      evolution of the southern Omineca belt. *Journal of structural geology, 24(6), 1195-1214.*
- 1312      Schrijver, K., 1973. Correlated changes in mineral assemblages and in rock habit and fabric across an  
1313      orthopyroxene isograd, Grenville Province, Quebec. *American Journal of Science, 273(2), 171-186.*
- 1314      Schwerdtner, W.M., Rivers, T., Zeeman, B., Wang, C.C., Tsolas, J., Yang, J., Ahmed, M. 2014. Post-  
1315      convergent structures in lower parts of the 1090–1050 Ma (early-Ottawan) thrust-sheet stack,  
1316      Grenville Province of Ontario, southern Canadian Shield. *Canadian Journal of Earth Sciences, 51(3),*  
1317      *243-265.*

- 1318 Sláma, J., Košler, J., Condon, D.J., Crowley, J.L., Gerdes, A., Hanchar, J.M., Horstwood, M.S.A., Morris,  
1319 G.A., Nasdala, L., Norberg, N., Schaltegger, U., Schoene, B., Tubrett, M.N., Whitehouse, M.J., 2008.  
1320 Plešovice zircon — A new natural reference material for U-Pb and Hf isotopic microanalysis. *Chemical*  
1321 *Geology*, 249(1), 1-35.
- 1322 Snoke, A.W., Tullis, J., Todd, V.R., 1998. *Fault-related Rocks: A Photographic Atlas*. Princeton: Princeton  
1323 University Press, 613 pp.
- 1324 Spear, F.S., 1993. *Metamorphic phase equilibria and pressure-temperature-time paths*. Washington,  
1325 D.C.: Mineralogical Society of America, 799 pp.
- 1326 Spear, F.S., 2004. Fast cooling and exhumation of the Valhalla metamorphic core complex, southeastern  
1327 British Columbia. *International Geology Review*, 46(3), 193-209.
- 1328 Spear, F.S., Florence, F.P., 1992. Thermobarometry in granulites: pitfalls and new approaches.  
1329 *Precambrian Research*, 55(1), 209-241.
- 1330 Spear, F.S., Kohn, M.J., Cheney, J.T., 1999. P-T paths from anatexitic pelites. *Contributions to Mineralogy*  
1331 *and Petrology*, 134(1), 17-32.
- 1332 Spear, F.S., Parrish, R.R., 1996. Petrology and cooling rates of the Valhalla Complex, British Columbia,  
1333 Canada. *Journal of Petrology*, 37(4), 733-765.
- 1334 Storm, L.C., Spear, F.S., 2005. Pressure, temperature and cooling rates of granulite facies migmatitic  
1335 pelites from the southern Adirondack Highlands, New York. *Journal of Metamorphic Geology*, 23(2),  
1336 107-130.
- 1337 Sullivan, W. A., & Snoke, A. W., 2007. Comparative anatomy of core-complex development in the  
1338 northeastern Great Basin, USA. *Rocky Mountain Geology*, 42(1), 1-29.
- 1339 Teyssier, C., Whitney, D.L., 2002. Gneiss domes and orogeny. *Geology*, 30(12), 1139-1142.
- 1340 Tirel, C., 2004. *Dynamique de l'extension des domaines continentaux épaissis: dômes métamorphiques et*  
1341 *écoulement de la croûte ductile* (Ph.D. thesis). Université de Rennes, Rennes, France, 252 pp.
- 1342 Tirel, C., Brun, J.P., Burov, E., 2004. Thermomechanical modeling of extensional gneiss  
1343 domes. *Geological Society of America Special Papers*, 380, 67-78.
- 1344 Tirel, C., Brun, J.P., Burov, E., 2008. Dynamics and structural development of metamorphic core  
1345 complexes. *Journal of Geophysical Research: Solid Earth*, 113(B04403), 1-25.
- 1346 Tirel, C., Brun, J.P., Sokoutis, D., 2006. Extension of thickened and hot lithospheres: Inferences from  
1347 laboratory modeling. *Tectonics*, 25(1), TC1005.
- 1348 Tracy, R.J., 1982. Compositional zoning and inclusions in metamorphic minerals. *Reviews in Mineralogy*  
1349 *and Geochemistry*, 10(1), 355-397.
- 1350 Tracy, R.J., Robinson, P., Thompson, A.B., 1976. Garnet composition and zoning in the determination of  
1351 temperature and pressure of metamorphism, central Massachusetts. *American Mineralogist*, 61,  
1352 762-775.
- 1353 Turner, G., Huneke, J.C., Podosek, F.A., Wasserburg G.J., 1971.  $^{40}\text{Ar}/^{39}\text{Ar}$  ages and cosmic ray exposure  
1354 age of Apollo 14 samples. *Earth and Planetary Science Letters*, 12(1), 19-35.
- 1355 Van Gool, J.A.M., Rivers, T., Calon, T., 2008. Grenville Front zone, Gagnon terrane, southwestern  
1356 Labrador: Configuration of a midcrustal foreland fold-thrust belt. *Tectonics*, 27(1), TC1104.
- 1357 Vanderhaeghe, O., Medvedev, S., Fullsack, P., Beaumont, C., Jamieson, R.A., 2003. Evolution of orogenic  
1358 wedges and continental plateaux: insights from crustal thermal-mechanical models overlying  
1359 subducting mantle lithosphere. *Geophysical Journal International*, 153(1), 27-51.

- Vielzeuf, D., Schmidt, M.W., 2001. Melting relations in hydrous systems revisited: application to metapelites, metagreywackes and metabasalts. *Contributions to Mineralogy and Petrology*, 141(3), 251-267.
- Villa, I.M., 1998. Isotopic closure. *Terra Nova*, 10(1), 42-47.
- Villa, I.M., Grobéty, B., Kelley, S.P., Trigila, R., Wieler, R., 1996. Assessing Ar transport paths and mechanisms for McClure Mountains Hornblende. *Contribution to Mineralogy and Petrology*, 126(1-2), 67-80.
- Villa, I.M., Puxeddu, M., 1994. Geochronology of the Larderello geothermal field: new data and the "closure temperature" issue. *Contributions to Mineralogy and Petrology*, 115(4), 415-426.
- Watson, E.B., Harrison, T.M., 2005. Zircon thermometer reveals minimum melting conditions on earliest Earth. *Science*, 308(5723), 841-844.
- Watson, E.B., Wark D.A., Thomas J.B., 2006. Crystallization thermometers for zircon and rutile. *Contribution to Mineralogy and Petrology*, 151(4), 413-433.
- Wernicke, B., 1985. Uniform-sense normal simple shear of the continental lithosphere. *Canadian Journal of Earth Sciences*, 22(1), 108-125.
- Winter, J.D., 2001. *An introduction to igneous and metamorphic petrology*. New York: Prentice Hall, 699 pp.
- Worley, B., Powell, R. 2000. High-precision relative thermobarometry: theory and a worked example. *Journal of Metamorphic Geology*, 18(1), 91-102.
- Yardley, B.W.D., 1977. An empirical study of diffusion in garnet. *American Mineralogist*, 62, 793-800.
- York, D., 1968. Least squares fitting of a straight line with correlated errors. *Earth and planetary science letters*, 5, 320-324.

## Figure Captions

Fig. 1. Simplified geologic map of the Mauricie area (modified from Nadeau and Brouillette, 1995). Age constraints on the Tawachiche and western Taureau shear zones are from Corrigan and van Breemen (1997) and Martignole and Friedman (1998). Opx-in isograd was drawn after Schriver (1973), and Hocq and Dufour (1999, 2002) following the descriptive definition of Carmichael (1978). Black rectangle represents study area shown on Fig. 2. Inset shows the simplified tectonic subdivisions of the Grenville Province (modified from Rivers, 2008) with the location of the Mauricie area (black rectangle). MT—Morin terrane, MTD—Mékinac-Taureau domain, SD—Shawinigan domain, PMD—Portneuf—Mauricie domain, PLD—Parc des Laurentides domain, MA—Anorthosite, SMF—St. Maurice fault.

Fig. 2. Simplified geologic map of the study area with location of samples used for thermobarometry, U-Pb geochronology and  $^{40}\text{Ar}/^{39}\text{Ar}$  thermochronology. Structural data (poles to foliation (circles) and lineations (X)) are divided according to structural domains delimited by dashed

lines. Stereonets are lower hemisphere equal area projections. Contours were produced with Stereonet software v.1.5 using the 1% area method and 2 sigma contour intervals (2-20 sigma) for stereonet containing more than 40 data points. Geologic map from Nadeau et al. 2009.

Fig. 3A. Panoramic view of the St-Tite gravel pit, a key outcrop where the eastern Taureau shear zone is best exposed and where samples RS11-098, RS11-089 and RS11-082 were collected. The inset is a sketch of the principal structures of the outcrop. Blue lines represent strongly deformed marble layers. Prime locations for the observation of top-down-to-the-ESE kinematic indicators are shown in red ( $\sigma$ - and  $\delta$ -porphyroclasts, asymmetric z-folds). Letters in the inset refer to the locations of close-up photographs, which have the same orientation unless specified otherwise. Lineation ( $L_{n+1}$ ) is plunging to the ESE (see structural subdomain 3 on Fig. 2), i.e. subparallel to the outcrop surface. B. Lower strain area indicated by the preservation of an earlier, folded, foliation  $S_n$  that is not completely transposed into the  $S_{n+1}$  foliation. C.  $\delta$ -porphyroclast of orthopyroxene. D.  $\sigma$ -porphyroclast of K-feldspar-rich leucosome pod. E. Foliation  $S_{n+1}$  of the host gneiss (H) entrained at the margins of an anastomosing marble layer (M).

Fig. 4. A. Composite microphotograph in cross polarized light (XPL) of a paragneiss located in the Mékinac-Taureau domain ~3km below the eastern Taureau shear zone (sample RS11-058). Syn-kinematic recrystallization of quartz ribbons forming an oblique grain-shape fabric suggests top-down-to-the-ESE sense of shear. Fine grain material within the quartz layer is a mixture of Sil + Bt + Kfs + Pl + Rt. B. Extensional ductile-brittle structure in the Shawinigan domain showing top-down-to-the-SE sense of shear. View is not perfectly parallel to the stretching lineation along the shear plane, which plunges towards the SE. These structures are interpreted as structurally higher equivalents of the Taureau shear zone that were active during waning stages of extension.

Fig. 5. Representative microphotographs of metapelite and amphibolite analyzed for thermobarometry. A. Typical metamorphic assemblage in metapelite RS11-105 of the Shawinigan domain containing Qtz + Kfs + Pl + Grt + Bt + Sil. This assemblage characterizes all metapelites from the Mauricie area. B. Perfectly euhedral garnet grains from the interior of the Mékinac-Taureau domain (sample RS11-021). C. Type 1 garnet containing abundant ilmenite inclusions (sample RS11-105). D. Type 2 garnet containing abundant quartz inclusions (sample RS11-105). E. Type 3 inclusion-poor garnet (sample RS11-105). F. View parallel to the lineation of an amphibolite with  $\sigma$ -shaped reaction rims of

plagioclase and hornblende around garnet (sample RS11-082B). Inset is a view perpendicular to the lineation at the same scale. Sigmoid shape of reaction rims implies that the reaction was pre- to syn-kinematic.

Fig. 6. Representative chemical composition profiles of garnet from core to rim. A Metapelite from the interior of the Mékinac-Taureau domain. B-C. Metapelite from the external zone of the Mékinac-Taureau domain. D-G. Metapelite from the Shawinigan domain. H. Amphibolite from the eastern Taureau shear zone. Notice the lack of zoning in garnet typical of retrograde net transfer reaction in migmatitic metapelites, such as spike in  $X_{\text{sps}}$  at the rim (Spear et al. 1999). See text for additional interpretation of the zonation.

Fig. 7. Pressure and temperature obtained from the Mékinac-Taureau and the Shawinigan domain with metapelites (A) and amphibolite (B). Samples are located on Fig. 2. Uncertainties for the metapelites are  $\pm 50$  °C and  $\pm 100$  MPa on temperature and pressure, respectively, as estimated by Essene (1989) and Berman (1991), and are represented by parallelograms based on the thermometric and barometric reactions. The amphibolite was used to calculate peak and retrograde conditions by combining all possible permutations of the mineral compositions data set. Pink stars show the averages of all permutations with a 95% confidence ellipse. Note that these errors do not include uncertainties stemming from the thermodynamic database nor from calculations of mineral activities. Results suggest high grade (820-880 °C; 1000-100 MPa) metamorphism in the Mékinac-Taureau domain overprinted by retrograde metamorphism (675-775 °C; 650-800 MPa) in the upper structural levels, whereas the Shawinigan domain was metamorphosed at conditions varying from 775 to 700 °C and from 850 to 625 MPa. See text for further explications. Ky-Sil transition is from Pattison (1992); wet solidus and Ms-out reaction are from Vielzeuf and Schmidt (2001) and references therein; compositional dependant Bt-out reactions are from phase equilibria modeling of a typical metapelite (Brown, 2010; B10) and from the partial melting experiment of a two-micas pelite (Patino Douce and Johnson, 1991; PDJ91). The prograde equivalent of the net transfer reaction (7),  $\text{Bt} + \text{Sil} + \text{Pl} + \text{Qtz} = \text{Grt} + \text{Kfs} + \text{melt}$ , operates once the Ms-out reaction is crossed and as long as all reactants are present in the rock (i.e. until the Bt-out reaction).

Fig. 8. Syn-kinematic pegmatite (sample RS11-098) cross-cutting the host rock foliation, but locally containing a weak internal foliation parallel to the external foliation  $S_{n+1}$ . "C-S" fabric above the main



pod (Fig. 8B) and dragging of the host gneiss foliation indicate top-down-to-the-ESE sense of shear. Rectangle shows the location of Fig. 8B. Inset outlines the major contacts between the pegmatite and the host rock. B. C-S fabric indicating syn-kinematic emplacement of the pegmatite. S-planes are defined by the host rock foliation and pegmatite dykelets define C-planes. Also note the  $\sigma$ -porphyroclast (P) of clinopyroxene partially replaced by hornblende, indicating retrograde metamorphism prior to or during shearing.

Fig. 9. A. Cathodoluminescence images of representative zircon from sample RS11-098. Group 1 zircon is commonly overgrown by Group 2 and rarely by Group 3 zircon, but no physical relationship is observed between Groups 2 and 3. Group 1 zircon is interpreted as primary igneous zircon, Groups 2 and 3 as metamorphic zircon, and Group 4 as inherited zircon. Circles are spots analyzed for geochronology. Their diameters are 25  $\mu\text{m}$  large except for spots outlined in white, which are 30  $\mu\text{m}$ . B. Cathodoluminescence images of representative zircon crystals from sample RS12-040. Prismatic shape and oscillatory zoning of zircon from this sample are typical of igneous crystallization. Analyzed spots are 25  $\mu\text{m}$  large.

Fig. 10. A-D. Geochemical composition diagrams showing differences and similarities between Groups 1-4 zircon from sample RS11-098. Similar chemical composition between Groups 1 and 2 and depletion of non-essential structural constituent cations (ex: U, Th, REE) in Group 2 as compared to Group 1, suggest that Group 2 zircon is derived from dissolution and reprecipitation of Group 1 zircon (Hoskin and Black, 2000; Hoskin and Schaltegger, 2003). Group 3 zircon has a distinct chemical composition that suggests an origin from a distinct fluid. Group 4 zircon includes inherited cores that do not match the composition and/or age of Group 1-3 zircon. See text for details.

Fig. 11. Weighted mean  $^{207}\text{Pb}/^{206}\text{Pb}$  dates for A-C. syn-extension pegmatite RS11-098 (UTM 680719E, 5178838N, NAD 83, zone 18N) and D. post metamorphic peak pegmatite RS12-040 (UTM 674542E, 5172883N, NAD 83, zone 18N). Error on individual dates are given at  $2\sigma$  and do not include the standard calibration uncertainty. Error on weighted mean (grey boxes) are given at  $2\sigma$  upon propagation of the standard calibration uncertainties. Weighted mean  $^{207}\text{Pb}/^{206}\text{Pb}$  dates are preferred for interpretations because they are more precise than U/Pb dates upon propagation of standard calibration uncertainties and because they are not affected by recent Pb loss. MSWD—mean square weighted deviation, PF—probability of fit, n—number of analyses, Ti-in-Zrn—Temperature of

crystallization based on the Ti-in-zircon thermometer (Ferry and Watson, 2007; Watson et al. 2006). Isotope ratios, ages, chemical composition and temperature of crystallization for any single analysis can be found in supplementary data table 2.

Fig. 12.  $^{39}\text{Ar}/^{40}\text{Ar}$  age spectra for A. amphibole and biotite of sample RS11-002; B. amphibole and biotite of sample RS11-115; C. biotite of sample RS11-015; D. amphibole of sample RS11-089; E. amphibole and biotite of sample RS11-113; F. biotite of sample RS11-105. The age error bars for each temperature steps are at the  $1\sigma$  level. Plateau and pseudo-plateau ages ( $2\sigma$  uncertainties) are given when applicable. See text for interpretations. Samples are located on Fig. 2.

Fig. 13. Compilation of thermobarometric, thermochronologic and geochronologic results placed on a schematic cross-section of the southeastern Mékinac-Taureau and Shawinigan domains. Samples are located on Fig. 2 and their structural positions (in km) is projected perpendicular to the eastern Taureau shear zone.  $^{40}\text{Ar}/^{39}\text{Ar}$  cooling ages are defined by plateau ages, except for sample RS11-113 (Hbl) that is defined by a pseudo-plateau. U-Pb dates ( $^{207}\text{Pb}/^{206}\text{Pb}$  on zircon) provide a minimum age for regional deformation and peak metamorphism (RS12-040) and an age of significant shearing along the eastern Taureau shear zone (RS11-098). See text for further details and interpretation.

Fig. 14. A. Simplified geologic map of lithotectonic domains and major shear zones of the Mauricie area (modified from Nadeau and Brouillette, 1995). Cross section A-A' is shown in Fig. 14C. B. Schematic structural profile representing the configuration of thrust-imbricated domains prior to extension. This configuration might have prevailed before  $1082 \pm 20$  Ma, the minimal age constraint determined for peak metamorphism and thrusting in the Mékinac-Taureau domain. The vertical pressure scale is based on values obtained from the Mékinac-Taureau and Shawinigan domains and depth in kilometers is calculated assuming a pressure gradient of 30 MPa/km (Winter, 2001). Red pods represent leucosome material at the Mékinac-Taureau and Shawinigan domains interface. The approximate trace of the future detachment zone (i.e. the eastern Taureau and Tawachiche shear zones) is shown on the cross-section. C. A-A' cross-section showing the architecture after the 1065-1035 Ma episode of extension, modified after Rivers (2012) and Rivers et al. (2012). Deformation was localized along both the eastern Taureau and Tawachiche shear zones, responsible for the exhumation of the Mékinac-Taureau and Shawinigan domains as a metamorphic core complex. Reference points (blue stars) show how different crustal levels were juxtaposed laterally. WTSZ—western Taureau shear zone, ETSZ—eastern Taureau

1511 shear zone, TWSZ—Tawachiche shear zone.

1512 **Table captions**

1513 Table 1. Summary of chemical compositions from microprobe analyses and calculated P-T results.

1514 Table 2. Summary of  $^{40}\text{Ar}/^{39}\text{Ar}$  results.

1515 **Supplementary data repository captions**

1516 Supplementary U-Pb and  $^{40}\text{Ar}/^{39}\text{Ar}$  geochronology analytical methods.

1517 Supplementary data table 1. Mineral compositions determined by electron microprobe analysis.

1518 Supplementary data table 2. U-Pb isotopic compositions and trace element concentrations.

1519 Supplementary data table 2.  $^{40}\text{Ar}/^{39}\text{Ar}$  data.

1520 Supplementary Fig. S1. Concordia diagrams for Groups 1-3 zircon of pegmatite RS11-098. D.  
1521 Concordia diagram for zircon of pegmatite RS12-040. Individual error ellipses are at  $2\sigma$  level and do not  
1522 include standard calibration uncertainties. Dates are  $^{207}\text{Pb}/^{206}\text{Pb}$  weighted averages and errors are at  $2\sigma$   
1523 level, including standard calibration uncertainties.

- 1 We conducted thermobarometry and geochronology on samples of the Mauricie area.
- 2 Peak metamorphism (~1000-1100 MPa and ~820-880 °C) occurred prior to  $1082 \pm 20$  Ma.
- 3 A top-down-to-the-ESE shear zone is responsible for exhumation at  $\sim 1064 \pm 15$  Ma.
- 4 Shearing was coeval with retrograde metamorphism.
- 5 A metamorphic core complex was formed by orogenic collapse in fixed-boundary mode.

Table 1. Summary of chemical compositions from microprobe analyses and calculated P-T results

		Interior of the MTD <sup>a</sup>			External zone of the MTD <sup>a</sup>			Shawinigan domain		
		RS12-021	RS11-058	RS12-015A	RS12-027B	RS11-105 T.1 <sup>b</sup>	RS11-105 T.2 <sup>b</sup>	RS11-105 T.3 <sup>b</sup>		
Easting <sup>c</sup> Northing <sup>c</sup>		665301	671660	671945	667294	670199	670199	670199		
		5180591	5174314	5175942	5153813	5158530	5158530	5158530		
Fe/(Fe+Mg) <sup>d</sup>	core	63-65	69-70	64-66	73	79-80	80-81	81		
	rim	63-65	74-78	65-72	75-79	84-87	82-86	83-86		
	$\Delta\text{max}^f$	0	<+8	<+6	<+6	<+7	<+5	<+5		
Grt	$X_{\text{grs}}^d$	8-9	5-6	1-2	6-7	3-4	3	3		
	rim	7-8	5-6	2	5-6	3	3	3		
	$\Delta\text{max}^f$	<1	0	<+1	<2	<1	0	0		
	core	1	2-3	<1	<1	2	2	2		
	rim	1	2-3	<1	<1	2-3	2-4	3		
	$\Delta\text{max}^f$	0	0	0	0	<+1	<+2	<+1		
Bt	arm. <sup>g</sup>	36-39	40-44	36-40	47-48	53-56	53-56	53-56		
	ct. <sup>g</sup>	31-33	36-37	26-34	40-47	51-54	51-54	51-54		
	arm. <sup>g</sup>	0.15-0.18	0.14-0.15	0.14-0.18	0.14-0.18	0.14-0.17	0.14-0.17	0.14-0.17		
	ct. <sup>g</sup>	0.13-0.18	0.13-0.15	0.12-0.15	0.13-0.15	0.11-0.15	0.11-0.15	0.11-0.15		
Pl	An	43.3-45.8	37.2-41.3	7.8-20.3	32.4-39.8	20.5-22.2	20.5-22.2	20.5-22.2		
P <sup>g</sup>	MPa	1050-1120	780-790	N/A	740-790	720-860	620-650	640		
T <sup>g</sup>	°C	820-850	780	740-780	780	730-750	700-710	700-710		

## Notes

- a) MTD: Mékinac-Taureau domain  
b) RS11-105 results are given for types 1-3 garnet (T.1; T.2; T.3, respectively)  
c) UTM NAD 83, zone 18N  
d)  $X_{\text{alm}}, X_{\text{prp}}, X_{\text{grs}}, X_{\text{sps}}, \text{Fe}/(\text{Fe}+\text{Mg})$  and are given as %  
e) Ti concentration is given as cation number per formula unit (p.f.u.) based on 6 oxygens formula.  
f)  $\Delta\text{max}$  represents the largest variation between the chemical composition of the core and the rim. "+" is an increase, "-" is a decrease.  
g) arm.: armoured; ct.: contact with garnet; P.: pressure; T: temperature.

Table 1. Continued

			Eastern Taureau shear zone RS11-082B
Easting <sup>a</sup>			680747
Northing <sup>a</sup>			5178829
Grt	Fe/(Fe+Mg) <sup>b</sup>	core	71-79
		inner rim	74-75
		outer rim	74-76
	X <sub>grs</sub> <sup>b</sup>	core	18-30
		inner rim	27-32
		outer rim	18-20
	X <sub>sps</sub> <sup>b</sup>	core	2-4
		inner rim	2-3
		outer rim	4-5
	Fe/(Fe+Mg) <sup>b</sup>	groundmass	43-45
		reaction rim	40-44
Pl	An	groundmass	40.2-50.7
		reaction rim	48.5-58.0
P <sup>c</sup>	MPa	peak <sup>d</sup>	990
		retro <sup>d</sup>	650
T <sup>c</sup>	°C	peak <sup>d</sup>	880
		retro <sup>d</sup>	720

**Notes**

a) UTM NAD 83, zone 18N

b) X<sub>alm</sub>, X<sub>prp</sub>, X<sub>grs</sub>, X<sub>sps</sub>, Fe/(Fe+Mg) and are given as %

c) T: temperature; P : pressure

d) peak: metamorphic peak; retro: retrograde metamorphism

**Table 2. Summary of  $^{40}\text{Ar}/^{39}\text{Ar}$  results**

Sample	Easting <sup>a</sup>	Northing <sup>a</sup>	Mineral dated	Age <sup>b</sup> (Ma)	$\pm 2\sigma$ (Ma)	% <sup>39</sup> Ar <sub>K</sub> defining plateau
<b>Core of the Mékinac-Taureau domain (12 and 8 km below the ETSZ)</b>						
RS11-002	657793	5196510	Hbl	998.6	7.4	85.8
RS11-002	657793	5196510	Bt	923.2	7.0	96.5
RS11-115	666117	5191538	Hbl	1010.0	7.4	93.4
RS11-115	666117	5191538	Bt	969.8	7.2	74.8
<b>External zone of the Mékinac-Taureau domain (3 km below the ETSZ)</b>						
RS11-015	671176	5177599	Bt	926.1	7.0	88.2
<b>Eastern Taureau shear zone (within the ETSZ)</b>						
RS11-089	680697	5178880	Hbl	1031.6	7.6	86.4
<b>Shawinigan domain (2 and 4 km above the ETSZ)</b>						
RS11-113	685301	5177182	Hbl	1022.3	7.6	49.2
RS11-113	685301	5177182	Hbl (pert. <sup>c</sup> )	1012.3	8.0	13.6
RS11-113	685301	5177182	Bt	930.4	7.0	79.3
RS11-105	670199	5158530	Bt	905.8	6.8	83.1

**Notes**

a) UTM NAD 83, zone 18N

b) all dates are plateau ages except for RS11-113 Hbl

c) pert. : thermal perturbation pseudo-plateau.

